Received Date: 02-May-2016

Revised Date: 31-Oct-2016

Accepted Date: 14-Dec-2016

Article Type: Research Article

# CT Breast Dose Reduction with the Use of Breast Positioning and Organ-Based Tube Current Modulation

**Wanyi Fu**

Department of Electrical and Computer Engineering

Carl E. Ravin Advanced Imaging Laboratories, Department of Radiology

Duke University, Durham, North Carolina 27705

**Xiaoyu Tian**

Department of Biomedical Engineering

Carl E. Ravin Advanced Imaging Laboratories, Department of Radiology

Duke University, Durham, North Carolina 27705

**Gregory Sturgeon**

Carl E. Ravin Advanced Imaging Laboratories, Department of Radiology

Duke University, Durham, North Carolina 27705

Greeshma Agasthya

Carl E. Ravin Advanced Imaging Laboratories, Department of Radiology

Duke University, Durham, North Carolina 27705

William Paul Segars

Department of Biomedical Engineering

Carl E. Ravin Advanced Imaging Laboratories, Department of Radiology

Duke University, Durham, North Carolina 27705

Mitchell M. Goodsitt

Department of Radiology

University of Michigan, Ann Arbor, Michigan 48109

Ella A. Kazerooni

Department of Radiology

University of Michigan, Ann Arbor, Michigan 48109

Ehsan Samei[a)]

Carl E. Ravin Advanced Imaging Laboratories, Department of Radiology

Medical Physics Graduate Program

Departments of Physics, Biomedical Engineering, and Electrical and Computer Engineering

[a)] Author to whom correspondence should be addressed. Electronic mail: samei@duke.edu



## ABSTRACT

**Purpose:** This study aimed to investigate the breast dose reduction potential of a breast positioning (BP) technique for thoracic CT examinations with organ-based tube current modulation (OTCM).

**Methods:** This study included 13 female anthropomorphic computational phantoms (XCAT, age range: 27 - 65 y.o., weight range: 52 - 105.8 kg). Each phantom was modified to simulate three breast sizes in standard supine geometry. The modeled breasts were then morphed to emulate BP that constrained the majority of the breast tissue inside the 120° anterior tube current (mA) reduction zone. The OTCM mA value was modeled using a ray-tracing program, which reduced the mA to 20 % in the anterior region with a corresponding increase to the posterior region. The organ doses were estimated by a validated Monte Carlo program for a typical clinical CT system (SOMATOM Definition Flash, Siemens Healthcare). The simulated organ doses and organ doses normalized by $CTDI_{vol}$ were used to compare three CT protocols: attenuation-based tube current modulation (ATCM), OTCM, and OTCM with BP ($OTCM_{BP}$).

**Results:** On average, compared to ATCM, OTCM reduced the breast dose by 19.3 ± 4.5 %, whereas $OTCM_{BP}$ reduced breast dose by 38.6 ± 8.1 % (an additional 23.8 ± 9.4 %). The dose saving of $OTCM_{BP}$ was more significant for larger breasts (on average 33, 38, and 44% reduction for 0.5, 1, and 2 kg breasts, respectively). Compared to ATCM, $OTCM_{BP}$ also reduced thymus and heart dose by 15.1 ± 7.4 % and 15.9 ± 6.2 %, respectively.

**Conclusions:** In thoracic CT examinations, OTCM with a breast positioning technique can markedly reduce unnecessary exposure to the radiosensitive organs in the anterior chest wall, specifically breast tissue. The breast dose reduction is more notable for women with larger breasts.

**KEYWORDS**: thoracic CT, Monte Carlo, organ dose, breast dose, organ based tube current modulation

## I. INTRODUCTION

Computed tomography (CT) has significantly benefitted the clinical diagnosis of a wide spectrum of diseases. In the past decades, the use of CT has grown exponentially. In 2014, approximately 81.2 million CT examinations were performed in the United States.[1, 2] The increased number of CT examinations has led to concerns about the associated population-based

radiation dose.[3] Significant efforts have been made to minimize unnecessary radiation exposure and maximize patient benefits through the development of dose reduction techniques.[4] These techniques generally aim to reduce the unnecessary exposure to major radiosensitive organs while maintaining the required image quality level.[5, 6]

Breasts are among the most radiosensitive organs for female patients.[7,8] In thoracic CT examinations, although breasts are usually not diagnostically targeted, they receive a considerable amount of radiation dose.[9-12] In an effort to protect superficial radiosensitive organs such as breasts, some vendors have developed organ based tube current modulation (OTCM) techniques.[13] In one implementation of OTCM, the tube current (mA) is reduced by 80 % in the anterior region (± 60°) of the patient with a corresponding increase in the posterior region (X-CARE, Siemens Healthcare). It has been reported that, with OTCM, breast doses can be reduced by 30 – 50 % with no detrimental effect on image quality.[5, 6, 14] However, a major challenge associated with the OTCM technique has been the extension of the breasts to outside the dose reduction zone.[15] A previous study has shown that, without any constraint, when the patient is supine, the breast tissue extends within an average angular zone of 155°; this is larger than the 120° dose reduction zone angle.[16] In effect, for most women, at least one breast partly resides in the increased dose zone, between ± 75° and ± 84°.[17] Another challenge with OTCM and associated breast dose is that the outer breast region contains a higher percentage of glandular tissue, making it more susceptible to cancer.[18] More than half of breast malignant tumors first develop in the upper outer quadrant of the breast.[19] As a result, the effectiveness of OTCM has been questioned, especially for women with larger breasts.[15]

The purpose of this study was to evaluate the dose reduction potential of a specially-designed breast positioning technique for OTCM examinations. The breast positioning technique was modeled by constraining most of the breast tissue to within the dose reduction zone. The dose reduction potential of this technique was evaluated across a library of phantoms with various ages, weights, and breast sizes. The organ doses were computed from Monte Carlo simulations with three CT scan protocols: attenuation based tube current modulation (ATCM), OTCM, and OTCM with breast positioning altered (referred to as $OTCM_{BP}$).

## II. MATERIAL AND METHODS

### A. Computational phantoms

This study included models of thirteen female adult patients (age range: 27-65 y.o., weight range: 52 to 105.8 kg) who received a chest and abdominal-pelvis, or a chest-abdominal-pelvis CT examination at our institution. The patients represented the anatomical variability amongst a clinical population with a broad range of age and BMI distribution (Figure 1).

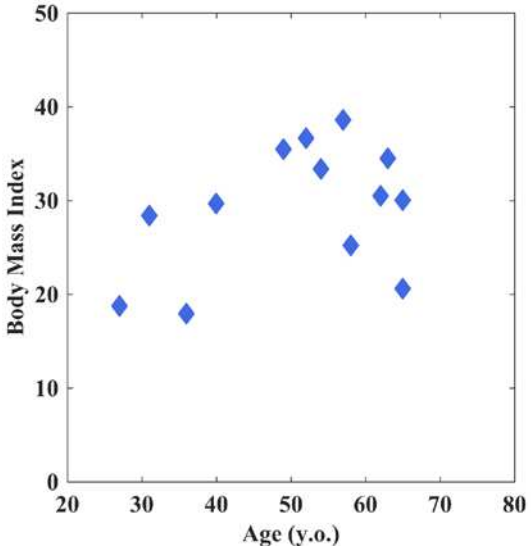


Figure 1: The BMI and age distribution of the computational phantoms

The models have been developed from the CT images of the patients.[20] Initially, large organs within the scan volumes were segmented to generate phantom masks followed by 3D triangulated polygon models using a marching cubes algorithm. The polygon structure was translated to 3D non-uniform rational B-spline surface (NURBS) (Rhinoceros, McNeel North America, Seattle, WA). The remaining organs and structures were generated by morphing a template's corresponding anatomies. The template was segmented from high-resolution visible human female full-body images.[21, 22] The organ volume was rescaled to the organ volume and anthropometry data reported in ICRP 89.[23] The phantoms frontal views are shown in Figure 2.

Each phantom was voxelized at an isotropic resolution of 3.45 mm for input into a Monte Carlo simulation program. The resolution was chosen considering the anatomic details and simulation time.[24]

To investigate the effect of dose on glandular density, two compositions of breasts were simulated: (1) 50/50 breast (50 % glandular tissue and 50 % adipose tissue), as a representative case for younger women and (2) 20/80 breast (20 % of glandular tissue and 80 % adipose tissue), which was an approximation of mean glandular percentage in a wide population.[25-27]

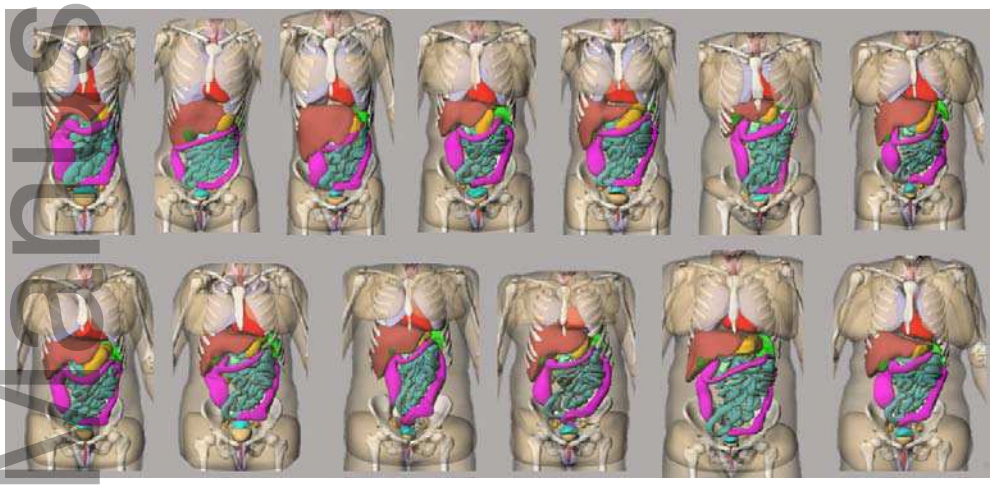

Figure 2: The three-dimensional frontal view of phantoms.

## B. Morphing the breasts

The phantom library was enhanced by modeling each phantom with two additional breast sizes (Figure 3). To allow for the use of additional breast sizes, the torso surface of each phantom was first modeled as a smooth breast-free surface. The individual breasts were modeled as closed surfaces that were added to the breast-free surface. The modeling of two additional breast geometries per patient providing a library of 39 phantoms preserved the breast-free surface and kept all other organs and structures constant.

Breast positioning (BP) was simulated on each phantom. The BP effectively modeled a support brassiere, which pressed breast tissue closer to the center of torso to a greater extent than a

normal brassiere. This ensured a majority of breast tissue within the ± 60° dose reduction zone. In order to approximate this BP numerically, finite element models of the breasts were created.[28] A voxelized version of each breast (at isotropic resolution of 0.2 mm) was used to create hexahedral finite elements for each voxel. The elements adjacent to the midline of the torso or the imaginary breast-free torso surface were constrained to have zero displacement. This restricted the overall motion of the breast and provided a consistent attachment to the remainder of the body during the deformation. The breasts were modeled as a uniform hyperelastic Neo-Hookean material with a moduli of elasticity (E_adipose 1 kPa), which has been previously used for breast FE simulations,[29-31] and a nearly incompressible Poisson's ratio of 0.49. The deformation due to the BP support was approximated as a body force roughly tangential to the breast-free torso surface, where the magnitude of the body force was scaled to achieve the desired positioning. The resulting large deformation finite element model was solved using FEBio (University of Utah's Musculoskeletal Research Laboratories and Columbia's Musculoskeletal Biomechanics Laboratory).[32] The force was applied incrementally using 20 equal steps to account for the large deformations.

Deformation fields from the finite element analysis were applied to transform the polygon meshes and subsequently NURBS surfaces of each breast. Manual corrections were applied, when necessary, to further morph the breasts to ensure that the desired positioning was achieved and that the breast volume remained constant. Figure 3 shows an example phantom with three breast sizes before and after applying BP. The phantom library was further divided into three groups by breast size: small (447 ± 187 g), medium (1068 ± 222 g), and large-sized (1929 ± 432 g) groups. The percentage of breast volume within dose reduction zone in standard supine positioning and after applying BP is listed in Table 1.

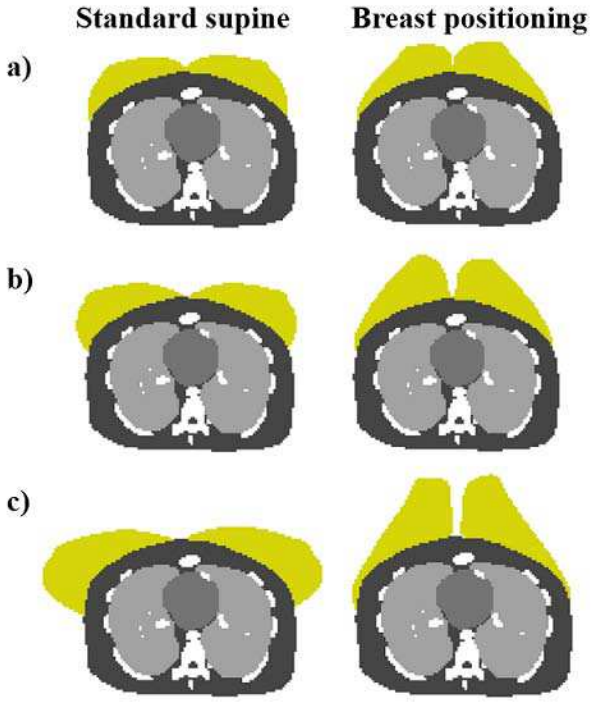


Figure 3: Transverse slice of a modified voxelized XCAT phantom. Three breast sizes are shown: (a) small, (b) medium (c) large with breast in standard supine position (left column) and the corresponding slice with breast positioning technique (right column). The breast tissue is highlighted in yellow.

Table 1: Mean of percentage of breast volume from all phantoms within ±60° frontal zone with and without breast positioning (BP).

| | Without BP (%) | With BP (%) | Change in Volume (%) |
|---|---|---|---|
| Small breasts | 68.5 ± 11.1 | 93.9 ± 4.2 | 25.5 ± 12.1 |
| Medium breasts | 68.0 ± 17.0 | 93.7 ± 5.2 | 25.6 ± 14.3 |
| Large breasts | 57.2 ± 14.5 | 93.9 ± 3.3 | 36.6 ± 12.3 |
| All Models | 64.6 ± 15.2 | 93.8 ± 4.0 | 29.1 ± 14.1 |

### C. CT examination simulations

A previously validated Monte Carlo simulation program was used to simulate CT scans.[27, 33] The package included PENOLOPE as a subprogram to track the energy loss of photons.[34, 35]

A 64-section CT system (SOMATOM Definition Flash; Siemens Healthcare, Forchheim, Germany) was modeled.[36] The scanner parameters were 120 kVp, pitch factor of 0.6, rotation time of 0.5 s, table speed of 2.304 cm/rot, 38.4 mm collimation, quality reference mAs of 150 mAs, and $CTDI_{vol}$ value denoted below. A clinical chest CT examination was simulated for each phantom. The scan coverage was defined as 1 cm above lung apex to 1 cm below the lung base.

The attenuation-based tube current modulation profile ($mA_{ATCM}$) simulated the virtual CAREDose4D, which takes into account attenuation of patient in both longitudinal (Z) and angular (XY) plane.[37] The XYZ attenuation through the phantom was simulated by a previously developed ray-tracing program.[24] At each projection angle θ, the 'fanbeam' function was used to measure the line integrals of attenuation coefficients alone each ray from the source to each detector bin (Matlab2010a; Mathworks, Natick, MA). The maximum line integrals of attenuation coefficients ($ud$) from all detector bins at $\theta$ was selected as the basis to generate tube current profile at $\theta$. The tube current profile was modeled as

$$mA_{ATCM}(\theta) = mA_0 e^{\alpha \times (ud(\theta))}, \quad (1)$$

where $mA_0$ and $mA_{ATCM}(\theta)$ are the fixed and attenuation modulated mA, respectively, $ud(\theta)$ is the maximum line integrals of attenuation coefficients calculated at $\theta$, and $\alpha$ is the modulation strength.[38] A typical averaged modulation strength level (α=0.5) was used. Finally, at each rotation angle, the tube current was scaled to below the systems' maximum mA limit.

To generate the organ based tube current profile ($mA_{OTCM}$) (X-CARE, Siemens Healthcare), the longitudinal (Z-plane) profile was reduced by 80 % between ± 60° and the reduction was evenly divided and added to the remaining projections within one rotation. The angular (XY-plane) modulation was turned off.[13] The longitudinal-profile was modeled as

$$mA_Z(\theta) = 0.5 \times (mA_0 e^{\alpha \times (ud(\theta_{AP}))} + mA_0 e^{\alpha \times (ud(\theta_{LAT}))}) \,, \quad (2)$$

where $mA_0$ and $mA_Z(\theta)$ are the fixed and longitudinal modulated mA, respectively, $ud(\theta_{AP})$ and $ud(\theta_{LAT})$ are the attenuation in AP (anterior-posterior) and in LAT (lateral) direction along the Z-plane at gantry angle $\theta$.[24] This approach emulated the CT system, in that the Z-profile was generated prior to the scan based on localization radiographs in LAT and AP directions.[24] The simulation further modeled gradual change in mA (slope as a function of rotation time, and upward- and downward-transition time) when switching between mA reduction and mA increase zone. Using 0.28 rot/s and 1 rot/s per Duan *et al.*,[13] the mA upward and downward times at 0.5 rot/s was estimated using linear approximation as 17 % and 6 % of rotation time, respectively. The mA value was generated for models with and without BP separately, thus, referred to as $mA_{OTCM}$ and $mA_{OTCM,BP}$, respectively. The $mA_{ATCM}$, $mA_{OTCM}$, and $mA_{OTCM,BP}$ of one example phantom is shown in Figure 4.

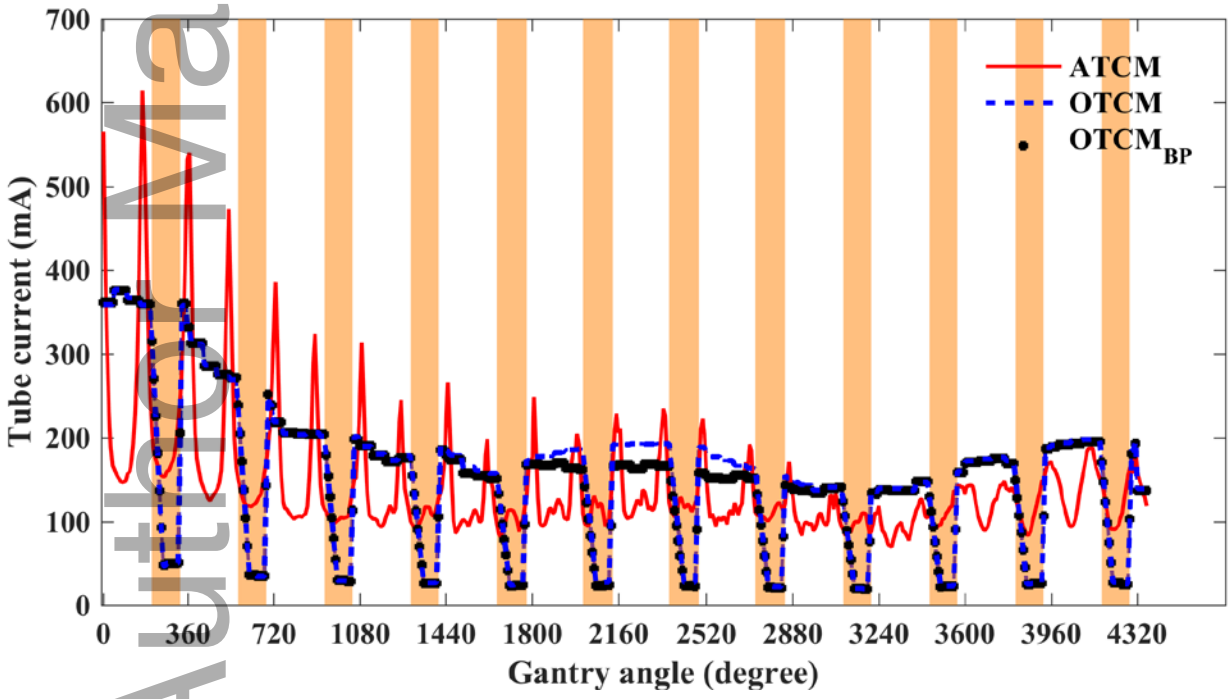


Figure 4: An example of the tube current profile generated for attenuation based tube current modulation (ATCM), organ-based tube current modulation (OTCM), and OTCM with breast positioning ($OTCM_{BP}$)

for a phantom with breast mass of 1098 g (50/50 breast) . The shaded regions correspond to the dose reduction zone.



## D. Organ dose estimation

Organ doses were determined by tracking the energy deposited within each organ using flux for a particular $CTDI_{vol}$ value specific to each phantom as dictated by the average mA over the scan coverage of the applied TCM. The $CTDI_{vol}$ values for the phantoms scanned with OTCM and ATCM ranged from 4.7 to 16.2 mGy. With breast positioning, $CTDI_{vol}$ changed slightly by an average of 4 ± 5 % reduction leading to a $CTDI_{vol}$ range of 4.5 to 17.1 mGy. The Size-Specific Dose Estimate (SSDE) was also calculated for each simulated scan using each phantom's chest water equivalent diameter[39] and the SSDE/$CTDI_{vol}$ conversion factors as defined by AAPM task group 204.[40] To report in detail, the $CTDI_{vol}$ and SSDE values for ATCM/OTCM and $OTCM_{BP}$ were fitted as an exponential function of chest water equivalent diameters (Figure 5). For $CTID_{vol}$, the fitting equations were $CTDI_{vol,ATCM/OTCM} = 0.56e^{0.09d}$ and $CTDI_{vol,OTCM_{BP}} = 0.49e^{0.1d}$ for ATCM/OTCM and $OTCM_{BP}$, respectively, where $d$ represents chest water equivalent diameter. For SSDE, the fitting equations were $SSDE_{ATCM/OTCM} = 2.12e^{0.06d}$ and $SSDE_{OTCM_{BP}} = 1.94e^{0.06d}$ for ATCM/OTCM and $OTCM_{BP}$, respectively. All fittings have $R^2 \geq 0.9$.

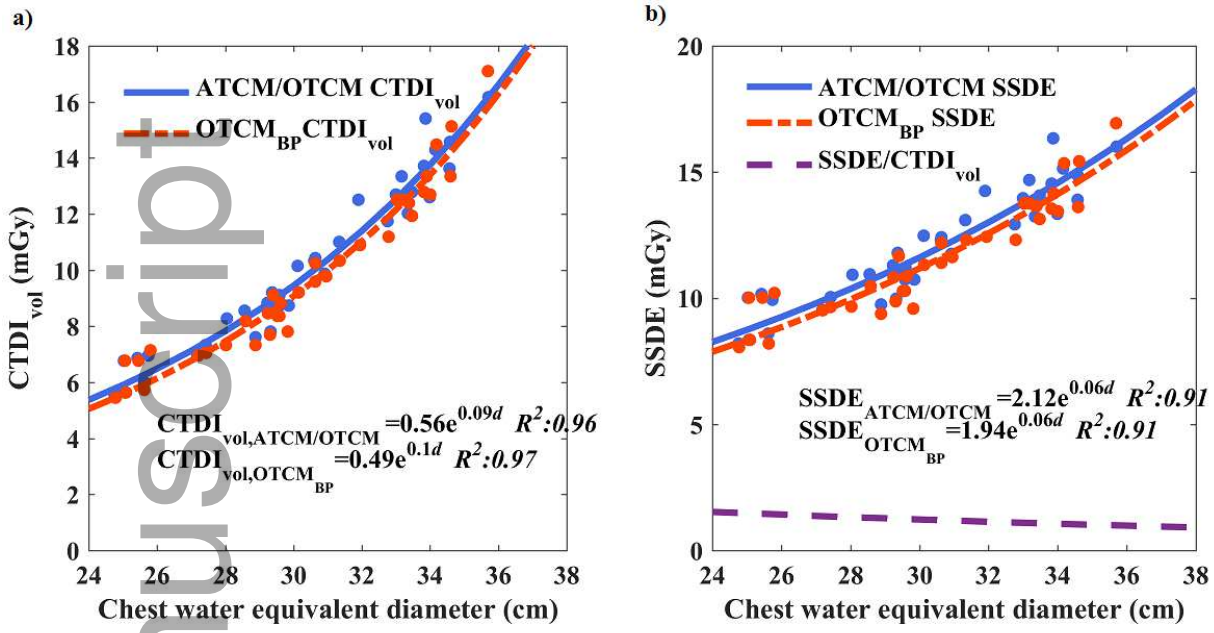


Figure 5: (a) $CTDI_{vol}$ and (b) SSDE values for ATCM/OTCM and $OTCM_{BP}$ scans fitted to chest water equivalent diameter.

The organ doses were further normalized by $CTDI_{vol}$ to derive the $CTDI_{vol}$-to-organ dose conversion coefficients (*h* factors). As $CTDI_{vol}$ alone significantly influences dose, expanding the results in terms of *h* factors could be interpreted as a comparing technique where total flux (and thus image quality by implication) remains constant, so that the net effect of modulation alone on dose can be evaluated by comparing $h_{ATCM}$ and $h_{OTCM}$. Similarly, the net effect of breast positioning alone can be evaluated by comparing $h_{OTCM}$ and $h_{OTCM,BP}$. The breast dose was computed for both 50/50 and 20/80 homogeneous breasts.

The organ dose and *h* factors percentage difference for breasts as well as other organs were calculated for OTCM, $OTCM_{BP}$ and ATCM, respectively. Organs were further grouped into anterior organs, medial or distributed organs, and posterior organs based on organ geometric center locations with respect to the CT scanner.

Because breast positioning repositions more breast volume within the dose reduction zone for larger breasts (Table 1), in order to assess the effect of breast mass on dose reduction potential, the breast dose value and *h* factors were further fitted to breast mass as

$$\widehat{D}_{breast} = p_{D,1} m_{breast} + p_{D,2} \quad (3a)$$

$$\hat{h}_{breast} = p_{h,1} m_{breast} + p_{h,2}, \quad (3b)$$

where $\widehat{D}_{breast}$ and $\hat{h}_{breast}$ denote the breast dose and $h$ factors for breasts, respectively, $m_{breast}$ is the weight of both breasts in each phantom, and $p_1$ and $p_2$ are the linear fitting coefficients.

To better estimate the overall organ dose reduction potential for OTCM and $OTCM_{BP}$, the average effective dose was calculated for ATCM, OTCM, and $OTCM_{BP}$. The effective dose was calculated as the sum of organ doses multiplied by tissue weighting factors defined by ICRP 103,[41] following the common practice of using effective dose as the scalar metric of radiation dose, even though, by definition, the effective dose can only be evaluated by reference phantoms. The doses for organs not explicitly modeled (salivary glands-, extrathoracic (ET) region-, oral mucosa-doses, lymphatic nodes- and muscle-doses), were approximated as the doses to neighboring organs.[33]

In order to report the organ dose, an exponential regression model of $h$ factors and chest diameter was calculated as

$$\hat{h} = e^{\alpha_h d + \beta_h}, \quad (4)$$

where $\hat{h}$ denotes the fitting curve of $h$ factors vs. chest diameter, $\alpha_h$ and $\beta_h$ are the fitting coefficients, and $d$ is the chest diameter. Given patient size, the organ dose can be rapidly predicted for this specific tube current modulation scheme and CT scanner.[36, 42 37, 43] Please note that this organ dose estimation technique is more accurate for organs within the scan coverage, where the majority of the dose is distributed.[38] Thus, given patient size and $CTDI_{vol}$, patient dose can be rapidly estimated for the CT system simulated in this study.

## III. RESULTS

On average, compared to ATCM, OTCM reduced the 50/50 breast dose by 19.3 ± 4.5 %. The average breast dose was further decreased by an additional 23.8 ± 9.4 % to 38.6 ±8.1 % with

$OTCM_{BP}$ compared to ATCM (Figure 6). The corresponding percentage reduction in terms of *h* factors were 21.3 ± 7.3 % ($OTCM_{BP}$ to OTCM) and 36.5 ± 6.9 % ($OTCM_{BP}$ to ATCM), respectively. Table 2 shows the average breast dose and *h* factors for the 50/50 and 20/80 breasts simulated with ATCM, OTCM and $OTCM_{BP}$. The difference in *h* factors between the two breast compositions was 8.8 ± 0.5 %, and the two compositions exhibited very similar trends in terms of impact of imaging method on dose. Figure 7 shows dose distribution plots of one phantom with small, medium, and large breasts undergoing ATCM, OTCM, and $OTCM_{BP}$ exams at a mid-transverse plane.

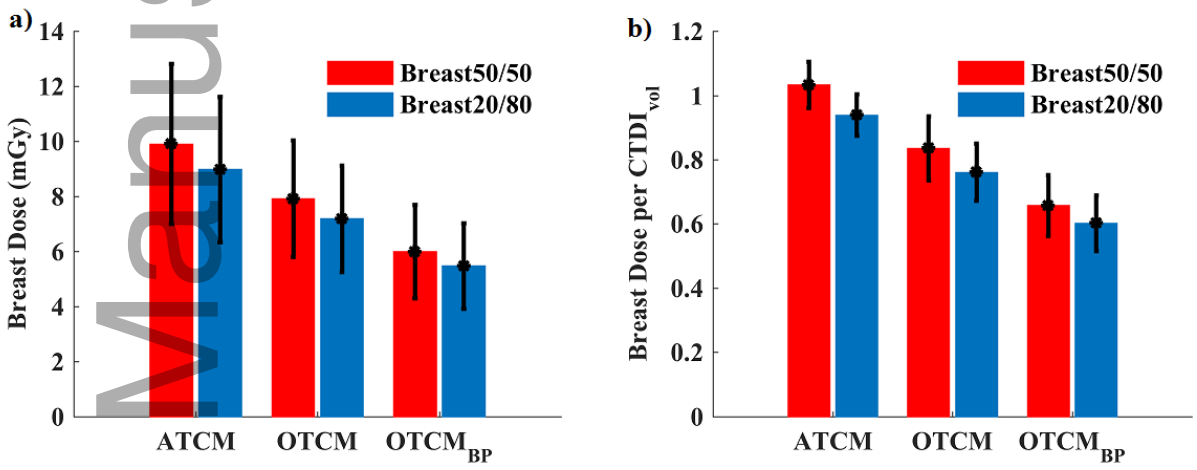


Figure 6: a) Breast dose and b) average of $CTDI_{vol}$-normalized-breast breast dose coefficients simulated with ATCM, OTCM, and $OTCM_{BP}$ for all phantoms with 50/50 and 20/80 breasts. Error bars represent ± 1 standard deviation.

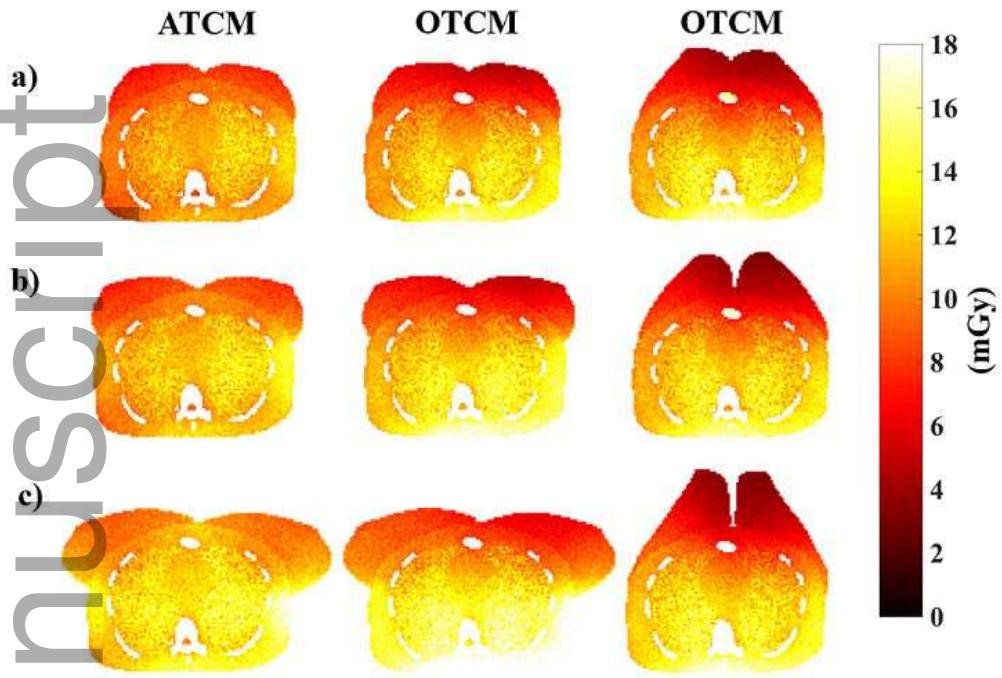


Figure 7: Dose distribution plots of one example phantom with small (a), medium (b), and large (c) breasts.

The breast dose saving of $OTCM_{BP}$ compared to ATCM was more significant for patients with larger breasts. For small (447 ± 187 g), medium (1068 ± 222 g), and large-sized (1929 ± 432 g) groups, $OTCM_{BP}$ and ATCM breast dose difference were -32.6 ± 7.0 %, -38.3 ± 5.2 %, and -44.8 ± 7.2 %. The corresponding values in terms of *h* factors difference were -31.4 ± 6.5 %, -36.8 ± 5.0 %, and -41.3 ± 5.3 %. respectively (Table 3). Compared to OTCM alone, $OTCM_{BP}$ breast dose decreased by 18.7± 9.0 %, 22.3 ± 7.1 %, and 30.5 ± 8.2 % for small, medium, and large sized groups, respectively. The corresponding value in terms of *h* factors were 17.3 ± 7.8 %, 20.4 ± 6.2 %, and 26.2 ± 4.9 %. The fitting coefficients of dose values vs. breast mass for the three protocols are given in Table 4 (Figure 8).

Table 2: Average breast dose and the difference from ATCM, OTCM, and $OTCM_{BP}$. [1]

| **Breast dose** | | | | | | |
|---|---|---|---|---|---|---|
| Breast Composition | ATCM Dose (mGy) | OTCM Dose (mGy) | $OTCM_{BP}$ Dose (mGy) | $OTCM_{BP}$ to ATCM difference (%) | OTCM to ATCM difference (%) | $OTCM_{BP}$ to OTCM difference (%) |
| 50/50 | 9.9 ± 2.9 | 7.9 ± 2.1 | 6.0 ± 1.7 | -38.6 ± 8.1* | -19.3 ± 4.5* | -23.8 ± 9.4* |
| 20/80 | 9.0 ± 2.6 | 7.2 ± 1.9 | 5.5 ± 1.6 | -38.1 ± 8.1* | -19.2 ± 4.5* | -23.4 ± 9.3* |
| **$CTDI_{vol}$-normalized-breast dose coefficients** | | | | | | |
| Breast Composition | ATCM Dose per $CTDI_{vol}$ | OTCM Dose per $CTDI_{vol}$ | $OTCM_{BP}$ Dose per $CTDI_{vol}$ | $OTCM_{BP}$ to ATCM difference (%) | OTCM to ATCM difference (%) | $OTCM_{BP}$ to OTCM difference (%) |
| 50/50 | 1.0 ± 0.1 | 0.8 ± 0.1 | 0.7 ± 0.1 | -36.5 ± 6.9* | -19.3 ± 4.5* | -21.3 ± 7.3* |
| 20/80 | 0.9 ± 0.1 | 0.8 ± 0.1 | 0.6 ± 0.1 | -36.0 ± 6.8* | -19.2 ± 4.5* | -20.8 ± 7.2* |

[1] Negative means dose reduction.
* represents statistical significant.

Table 3: Average breast dose coefficients and dose difference in different sized breast group. [2]

| **Breast dose** | | | | | | |
|---|---|---|---|---|---|---|
| Breast Size | ATCM Dose (mGy) | OTCM Dose (mGy) | $OTCM_{BP}$ Dose (mGy) | $OTCM_{BP}$ to ATCM difference (%) | OTCM to ATCM difference (%) | $OTCM_{BP}$ to OTCM difference (%) |
| Small | 8.0 ± 2.5 | 6.5 ± 1.8 | 5.4 ± 1.9 | -32.6 ± 7.0* | -16.9 ± 4.1* | -18.7 ± 9.0* |
| Medium | 9.3 ± 2.2 | 7.4 ± 1.6 | 5.8 ± 1.4 | -38.3 ± 5.2* | -20.5 ± 4.3* | -22.3 ± 7.1* |

| | | | | | | |
|---|---|---|---|---|---|---|
| Large | 12.4 ± 2.1 | 9.8 ± 1.5 | 6.8 ± 1.4 | -44.8 ± 7.2* | -20.6 ± 4.3* | -30.5 ± 8.2* |
| **$CTDI_{vol}$-normalized-breast dose coefficients** | | | | | | |
| Breast Size | ATCM Dose per $CTDI_{vol}$ | OTCM Dose per $CTDI_{vol}$ | $OTCM_{BP}$ Dose per $CTDI_{vol}$ | $OTCM_{BP}$ to ATCM difference (%) | OTCM to ATCM difference (%) | $OTCM_{BP}$ to OTCM difference (%) |
| Small | 1.1 ± 0.1 | 0.9 ± 0.1 | 0.7 ± 0.1 | -31.4 ± 6.5* | -16.9 ± 4.1* | -17.3 ± 7.8* |
| Medium | 1.0 ± 0.1 | 0.8 ± 0.1 | 0.6 ± 0.1 | -36.8 ± 5.0* | -20.5 ± 4.3* | -20.4 ± 6.2* |
| Large | 1.0 ± 0.1 | 0.8 ± 0.1 | 0.6 ± 0.1 | -41.3 ± 5.3* | -20.6 ± 4.3* | -26.2 ± 4.9* |

[2] Negative means dose reduction.

290 * represents statistical significant.

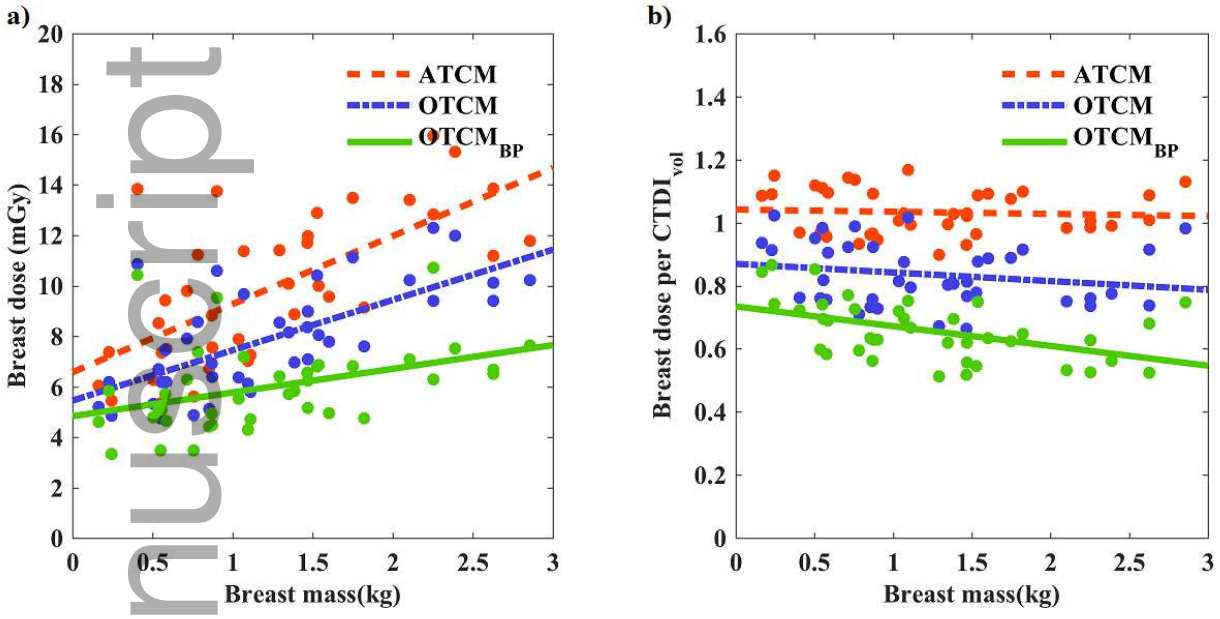


Figure 8: a) breast dose and b) $CTDI_{vol}$-normalized-breast dose coefficients linearly fitted to breast mass scanned with ATCM, OTCM and $OTCM_{BP}$ as equation (2).

Table 4: Fitting coefficients of breast dose and $CTDI_{vol}$-normalized-breast dose coefficients fitted vs. breast mass.

| | Breast dose | | | $CTDI_{vol}$-normalized-breast dose coefficients | | |
|---|---|---|---|---|---|---|
| | $p_{D,1}(kg^{-1})$ | $p_{D,2}$ | *RMSE* | $p_{h,1}(kg^{-1})$ | $p_{h,2}$ | *RMSE* |
| ATCM | 2.7 | 6.58 | 2.18 | -0.007 | 1.042 | 0.073 |
| OTCM | 1.99 | 5.45 | 1.57 | -0.027 | 0.87 | 0.098 |
| $OTCM_{BP}$ | 0.94 | 4.83 | 1.57 | -0.063 | 0.735 | 0.084 |

Figure 9 shows the organ dose differences between $OTCM_{BP}$ and ATCM, OTCM and ATCM, and $OTCM_{BP}$ and OTCM. Compared to ATCM, OTCM significantly reduced dose and *h* factors to general anterior organs (except larynx-pharynx) ( $p < 0.01$). Doses to several organs (large

intestine, stomach, thymus, pancreases, and small intestine) decreased up to 10 %. The doses to medial and posterior organ dose in OTCM compared to ATCM was increased by less than 10 % ( $p < 0.01$). For distributed organs such as bone-marrow and bone-surface, which are located more towards posterior of the patient, organ doses were increased by ~10 %. The skin dose remained relatively constant. When using BP compared to OTCM alone, all organ doses were decreased or not changed significantly. The corresponding *h* factors to anterior organs were decreased or not changed significantly and the *h* factors to medial and posterior organs were increased by less than 3 % (except for spleen).

Table 5 shows the average effective dose results for 39 phantoms and different breast-sized groups. The results showed that the effective doses were similar for ATCM and OTCM with 4.8 ± 1.1 mSv and 4.6 ± 1.0 mSv, respectively. ATCM to OTCM effective dose reduction was ~6 % for different breast-size groups. With BP, the average effective dose was reduced to 4.2 ± 1.0 mSv. Compared to ATCM, $OTCM_{BP}$ reduced effective dose by 11.2 ± 3.0 %, 12.4 ± 3.6 %, and 15.2 ± 6.0 % for small-, medium-, and large-sized breast groups, respectively.

Figure 10 shows *h* factors fitted to patient chest diameter as an exponential function and Table 6 shows the fitting coefficients. For organs within the scan coverage (lung, esophagus, heart, thymus, trachea-bronchi), the organ doses are more strongly correlated with chest diameters ($R^2 > 0.7$), except for breasts. For distributed organs, the correlations are moderate ($0.85 > R^2 > 0.6$). For organs on the periphery or outside of the scan coverage, the correlations are relatively small ($R^2 \leq 0.6$).

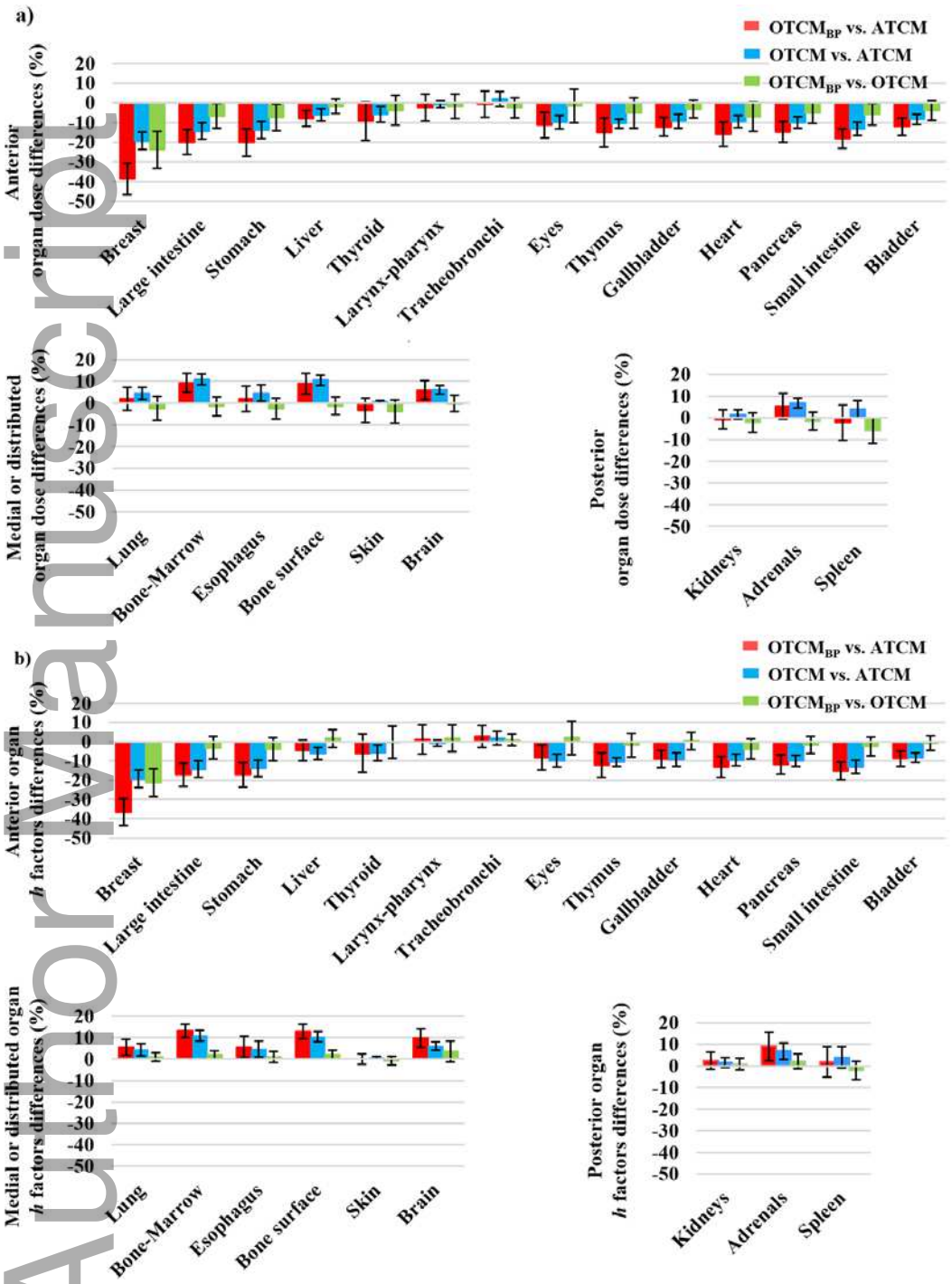


Figure 9: Differences in a) organ dose and b) $CTDI_{vol}$-normalized-organ dose coefficients across ATCM, OTCM and $OTCM_{BP}$.

Table 5: Average effective dose and the difference between ATCM, OTCM, and $OTCM_{BP}$. [1]

| Effective dose (ED) | | | | | | |
|---|---|---|---|---|---|---|
| Breast Size | ATCM ED (mSv) | OTCM ED (mSv) | $OTCM_{BP}$ ED (mSv) | $OTCM_{BP}$ to ATCM difference (%) | OTCM to ATCM difference (%) | $OTCM_{BP}$ to OTCM difference (%) |
| Small | 4.2 ± 1.1 | 3.9 ± 0.97 | 3.7 ± 1.0 | -11.2 ± 3.0* | -5.6 ± 1.7* | -5.9 ± 4.1* |
| Medium | 4.7 ± 0.88 | 4.5 ± 0.81 | 4.2 ± 0.87 | -12.4 ± 3.6* | -5.8 ± 1.9* | -7.0 ± 4.2* |
| Large | 5.6 ± 0.77 | 5.3 ± 0.71 | 4.8 ±0.78 | -15.2 ± 6.0* | -5.5 ± 1.4* | -10.3 ± 6.4* |
| All models | 4.8 ± 1.1 | 4.6 ± 1.0 | 4.2 ± 1.0 | -12.9 ± 4.6* | -5.6 ± 1.7* | -7.7 ± 5.2* |
| **ED normalized by dose-length-product (DLP)** | | | | | | |
| Breast Size | ATCM ED/DLP (mSv/mGy-cm) | OTCM ED/DLP (mSv/mGy-cm) | $OTCM_{BP}$ ED/DLP (mSv/mGy-cm) | $OTCM_{BP}$ to ATCM difference (%) | OTCM to ATCM difference (%) | $OTCM_{BP}$ to OTCM difference (%) |
| Small | 0.022 ± 0.002 | 0.021 ± 0.002 | 0.020 ± 0.001 | -9.8 ± 2.0* | -5.6 ± 1.7* | -4.4 ± 2.6* |
| Medium | 0.021 ± 0.002 | 0.020 ± 0.002 | 0.019 ± 0.002 | -10.3 ± 3.8* | -5.8 ± 1.9* | -4.8 ± 3.3* |
| Large | 0.020 ± 0.002 | 0.019 ± 0.002 | 0.018 ± 0.002 | -9.7 ± 2.3* | -5.5 ± 1.4* | -4.5 ± 1.6* |
| All models | 0.021 ± 0.002 | 0.020 ± 0.002 | 0.019 ± 0.002 | -9.9 ± 2.7* | -5.6 ± 1.7* | -4.6 ± 2.5* |

[1] Negative means dose reduction.
* represents statistical significant change.

Table 6: Fitting parameters of organ dose with respect to chest diameter [Eq. (4)]

| $CTDI_{vol}$-normalized-organ dose coefficients | | | | | | | | | |
|---|---|---|---|---|---|---|---|---|---|
| | ATCM | | | OTCM | | | $OTCM_{BP}$ | | |
| Organ | $\alpha_{h,ATCM}$ | $\beta_{h,ATCM}$ | $R^2$ | $\alpha_{h,OTCM}$ | $\beta_{h,OTCM}$ | $R^2$ | $\alpha_{h,OTCM,E}$ | $\beta_{h,OTCM,BP}$ | $R^2$ |
| Anterior organs | | | | | | | | | |
| Breast | -0.01 | 0.47 | 0.45 | -0.03 | 0.65 | 0.56 | -0.03 | 0.51 | 0.47 |
| Large intestine | 0.04 | -3.43 | 0.12 | 0.03 | -3.44 | 0.10 | 0.04 | -3.71 | 0.15 |
| Stomach | -0.05 | 1.05 | 0.31 | -0.05 | 0.96 | 0.30 | -0.04 | 0.44 | 0.20 |
| Liver | -0.03 | 0.36 | 0.46 | -0.03 | 0.25 | 0.38 | -0.02 | 0.12 | 0.28 |
| Thyroid | -0.08 | 1.85 | 0.53 | -0.07 | 1.51 | 0.53 | -0.05 | 0.85 | 0.41 |
| Larynx-pharynx | -0.01 | -1.09 | 0.09 | -0.01 | -1.18 | 0.06 | 0.00 | -1.51 | 0.00 |
| Trach-bronchi | -0.06 | 1.89 | 0.94 | -0.05 | 1.65 | 0.92 | -0.05 | 1.53 | 0.86 |
| Eyes | 0.01 | -4.55 | 0.09 | 0.00 | -4.39 | 0.01 | 0.02 | -4.82 | 0.16 |
| Thymus | -0.06 | 1.90 | 0.89 | -0.06 | 1.73 | 0.89 | -0.05 | 1.37 | 0.75 |
| Gallbladder | 0.01 | -2.17 | 0.02 | 0.01 | -2.16 | 0.01 | 0.01 | -2.26 | 0.02 |
| Heart | -0.05 | 1.43 | 0.86 | -0.05 | 1.33 | 0.82 | -0.04 | 1.00 | 0.71 |
| Pancreas | -0.03 | -0.32 | 0.09 | -0.03 | -0.45 | 0.09 | -0.02 | -0.78 | 0.04 |
| Small intestine | 0.03 | -3.26 | 0.08 | 0.03 | -3.24 | 0.06 | 0.03 | -3.51 | 0.11 |
| Bladder | -0.01 | -5.76 | 0.02 | -0.01 | -5.83 | 0.02 | -0.01 | -5.88 | 0.01 |
| Medial or distributed organs | | | | | | | | | |
| Lung | -0.04 | 1.35 | 0.87 | -0.04 | 1.26 | 0.84 | -0.04 | 1.25 | 0.81 |
| Bone marrow | -0.05 | 0.59 | 0.77 | -0.05 | 0.53 | 0.72 | -0.05 | 0.61 | 0.71 |
| Esophagus | -0.06 | 1.69 | 0.94 | -0.05 | 1.46 | 0.88 | -0.05 | 1.41 | 0.84 |
| Bone surface | -0.05 | 0.88 | 0.81 | -0.04 | 0.83 | 0.77 | -0.04 | 0.88 | 0.76 |
| Skin | -0.04 | -0.47 | 0.63 | -0.04 | -0.46 | 0.65 | -0.04 | -0.39 | 0.70 |
| Brain | -0.01 | -4.13 | 0.06 | -0.01 | -4.11 | 0.04 | -0.01 | -4.18 | 0.03 |
| Posterior organs | | | | | | | | | |
| Kidneys | -0.11 | 1.54 | 0.48 | -0.11 | 1.58 | 0.46 | -0.11 | 1.71 | 0.46 |
| Adrenals | -0.10 | 2.21 | 0.55 | -0.10 | 2.48 | 0.54 | -0.11 | 2.78 | 0.54 |
| Spleen | -0.05 | 0.99 | 0.40 | -0.04 | 0.83 | 0.29 | -0.03 | 0.64 | 0.22 |

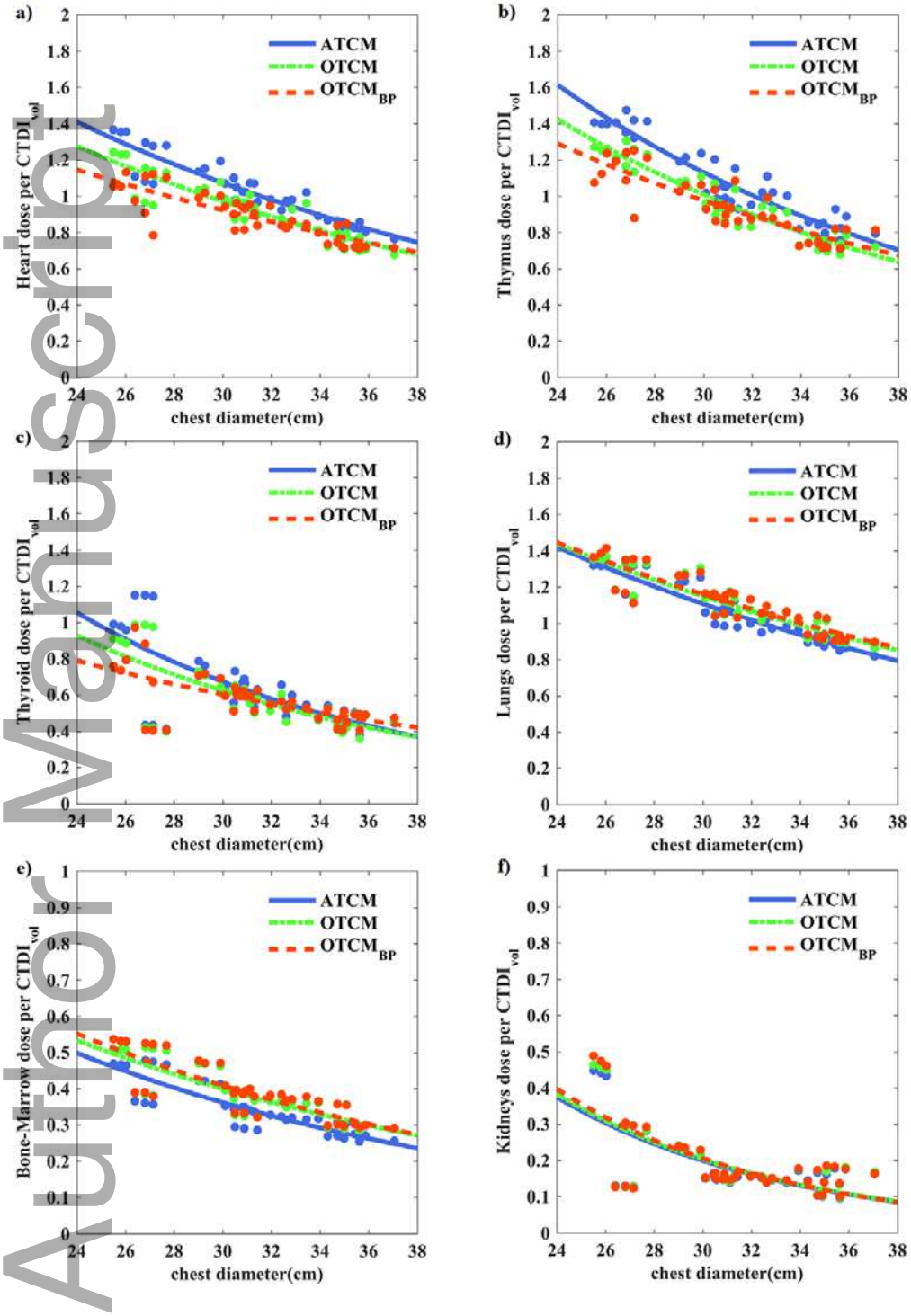

Figure 10: The $CTDI_{vol}$-normalized-organ dose coefficients fitted against phantom chest diameters as shown in Eq (4). Example organs from anterior (a-c), medial or distributed (d, e), and posterior (f) groups.

## IV. DISCUSSION

Organ-based tube current modulation techniques have been devised to minimize unnecessary radiation exposure to major radiosensitive organs while maintaining the required image quality. In this work, we evaluated the dose saving potential of an additional breast positioning technique for organ-based tube current modulation examinations (OTCM). Compared to standard tube current modulation, OTCM offered an average of 19.3 ± 4.5 % reduction in breast dose. The breast positioning extended that reduction by an additive 23.8 ± 9.4 %. Targeted breast positioning takes a fuller advantage of OTCM for reducing breast dose in body CT examinations. In this study, a constant $CTDI_{vol}$ value was used for ATCM and OTCM scheme for each phantom. A previous study has argued that OTCM is less dose-economical compared to ATCM, and resulted in a 5 – 10 % $CTDI_{vol}$ increase to maintain image quality.[14] When OTCM is utilized, the x-y modulation is shut off, the Z-plane mA is generated based on the average of AP and LAT attenuation. If techniques permit, keeping x-y plane modulation in OTCM would be more dose efficient. We simulated this scenario ($OTCM_{ideal}$), reducing $mA_{ATCM}$ by 80 % and a corresponding increase in the remaining projections. The dose reduction was larger in anterior organs. The dose for heart and thymus was reduced by 14.7 ± 3.4 % and 20.0 ± 4.6 %, respectively. The dose increase was smaller in distributed and posterior organs (except for spleen). No significant change was noted in lung, esophagus, and kidneys.

To take full advantage of OTCM, breast-positioning techniques constrain the breast to within the dose reduction zone. Seidenfuss *et al.* have demonstrated that a normal brassiere can constrain more breast tissue within the dose reduction zone.[44] However, in that implementation, the breasts are still not fully sheltered, especially in women with larger breasts where only 83.3 % of the volume is constrained. Additionally, that study did not evaluate the breast dose. In this study, we simulated the breast positioning technique that can optimize breast position beyond a normal brassiere's support by compressing more breast tissue to within the dose reduction zone. To

ensure the modeled breast locations reflect real scenario, the percentage of breast tissue within the dose reduction zone was compared with those reported in literature. Seidenfuss *et al.* reported breast volumes within dose reduction zone on CT images from 578 female patients with and without brassiere.[44] On average, 60.4 ± 24.7 % and 91.3 ± 9.4 % of breast volume was within dose reduction zone with and without a brassiere, respectively.[44] In our work, the average breast tissue within the dose reduction zone was 64.6 ± 15.2 % originally, and increased to 93.8 ± 4.0 % after applying BP. The ratio of breast within the dose reduction zone is higher in this study compared to Seidenfuss *et al.* because in our technique, the breast tissue was compressed closer towards the center of the torso. To implement the studied breast positioning technique clinically, we recommend the use of sports brassiere with foam padding.

The breast dose savings of OTCM and $OTCM_{BP}$ from ATCM were compared with physical phantoms reported by literature. Comparing OTCM to ATCM reduction for an anthropomorphic phantom with breast attachment, Lungren *et al.* reported the anterior and posterior breast dose reduction of 29 – 45 % and 9 – 19 %, respectively.[16] Our results were generally consistent; from ATCM to OTCM, the average breast dose reduction ranges at 11.0 - 28.7 %. For ATCM to $OTCM_{BP}$, the breast dose reduction ranges at 21.0 - 51.8 % and when normalized by $CTDI_{vol}$, the corresponding reduction ranges at 20.6% - 48.1 %. Another study reported that breast dose was reduced by 34 %, 34 %, and 39 % with OTCM compared to ATCM for small, medium, and large semi-anthropomorphic phantoms (30×20, 35×25, 40×30 cm in lateral and posterior-anterior dimension).[14] To derive breast dose corresponding to the above average chest diameter in our study, the breast dose was fitted to chest diameter as an exponential function [Eq. (4)] (Figure 11). On average, compared to ATCM, OTCM reduced breast dose by 13.1 %, 18.1 %, and 22.8 %, and *h* factors by 12.7 %, 18.0 %, and 23.0 %. The OTCM savings in our study was smaller compared to the literature, as the XCAT breasts were explicitly modeled, while the phantoms used in other studies were with "underdeveloped" breasts (i.e., the breasts were not spread).[6, 13, 14, 16, 45] Thus, more lateral portions of the XCAT breasts were in the dose-increased zone. The full advantage of OTCM was not taken without BP. The $OTCM_{BP}$ saved the breast dose by 34.4

%, 38.1 %, 41.5 % and *h* factors by 30.1 %, 35.3 %, and 40.2 % for phantoms with 25 cm, 30 cm, and 35 cm chest diameters, respectively.

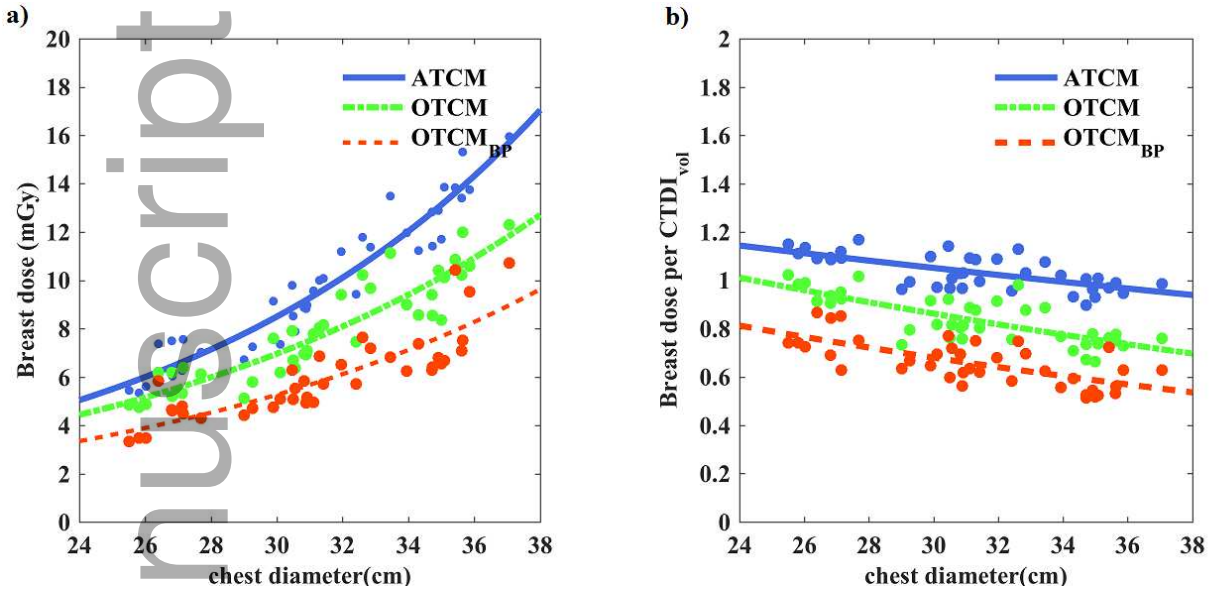


Figure 11: a) Breast dose and b) $CTDI_{vol}$-normalized-breast dose from ATCM, OTCM and $OTCM_{BP}$ simulations fitted to chest diameter as Eq (4).

Using the same $CTDI_{vol}$, OTCM reduced the effective dose slightly, this can be explained by the fact that most of the radiosensitive organs are located anteriorly.[46] Lungren *et al.* reported the effective dose by evaluating the organ dose recorded by dosimeters for an anthropomorphic physical phantom. The results were 4.41 ± 0.3 mSv (after scanning $CTDI_{vol}$ 6.94 mGy) and 5.25 ± 0.36 mSv (after scanning $CTDI_{vol}$ 7.51 mGy) for ATCM and OTCM, respectively.[16] The discrepancy between Lungren *et al.* and this study can be explained by the fact that the $CTDI_{vol}$ used in this study was constant between OTCM and ATCM, while the $CTDI_{vol}$ for OTCM is generally 5 – 10 % higher as noted previously.

Other organ doses were also compared with physical phantoms. Lungren *et al.* has reported anterior organ dose reduced 17 – 47 %; posterior organ dose significantly increased; lateral and inner organ dose showed similar results.[16] Our results were consistent on some typical anterior

and posterior organs. Thymus and kidney dose changed by 10.5 % and -1.6 % (7 % and -1 % from Lungren *et al.*). The skin dose profile was also compared with measurement of physical phantoms from the literature. The skin dose was sampled and interpolated within 360 degrees for each phantom on one selected slice that contains large volume of breast tissue. The interpolated skin dose was further averaged across all phantoms. Duan *et al.* reported surface dose of anthropomorphic phantoms receiving OTCM and fixed mA scan ($mA_{fix}$).[13] To compare our results to those of Duan et al., the skin dose was normalized by $CTDI_{vol}$ and scaled to unit average. Our results showed excellent agreement with the measurement from physical phantoms (Figure 12). For OTCM, the dose was unsymmetrical on left and right reduction zone, which was due to unequal upward and downward transition times. Compared to $mA_{fix}$, the $mA_{ATCM}$ is generally larger in LAT and smaller in AP.

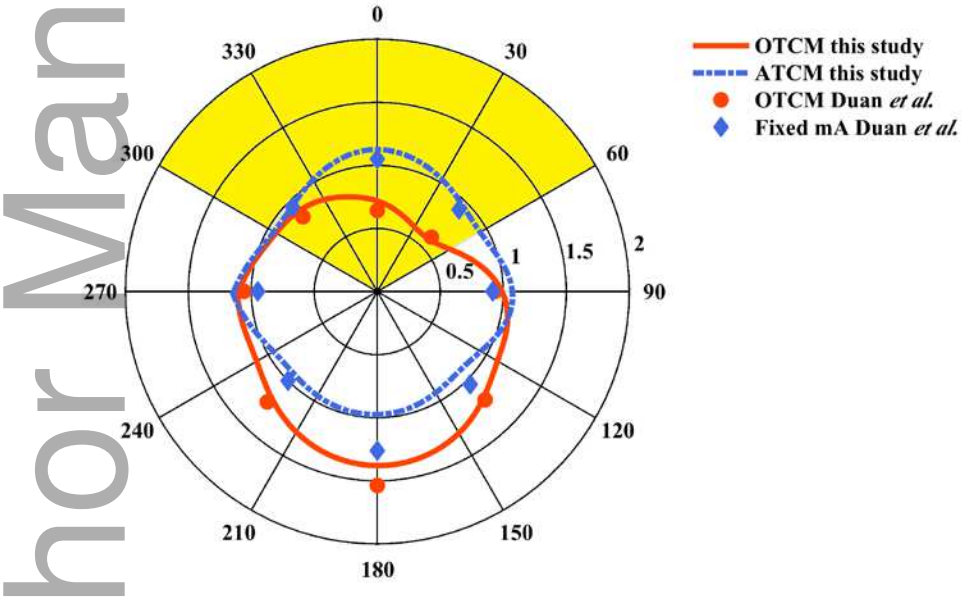


Figure 12: Skin dose simulated with computerized phantom with ATCM and OTCM from this study compared skin dose measured with physical phantoms with OTCM and fixed mA from Duan *et al.* The dose was averaged to a unit mean for comparisons. For this study, the skin dose profile was averaged across all phantoms. The dose reduction zone is shaded in yellow.

Although use of a patient's own brassiere is cost efficient, a specially designed BP support would be superior as it compresses more of the breast tissue within the dose reduction zone, especially the outer quadrant of the breast, which more than half of breast carcinoma occurs.[18, 19, 47] With a normal brassiere, 17 % of the breast is outside the dose reduction zone for large sized breasts.[44] With the implemented BP, the portion of breast tissue within the dose increased zone decreases to 6 %. Furthermore, BP constrains an average constant portion (94 %) of breast tissue within the dose reduction zone in all groups. However, normal brassieres performance varies among different breast-size groups.[44] The dose savings effect and potential artifacts in CT images with various normal brassieres is yet to be examined. A standardized BP allows one to accurately monitor dose and prospectively optimize CT procedure.

For all the organs within the scan coverage, lungs have the same radiosensitivity as breasts.[41] Our results showed that lung dose only increased slightly using OTCM, compared to ATCM. As the tube current was decreased anteriorly and increased posteriorly, the lung dose is non-uniformly distributed. To estimate the distribution of lung dose, lung dose was estimated at 5 different lung ROIs on the dose distribution plot located as shown in Figure 13. The lung dose was averaged over each ROI across 39 phantoms for each modulation scheme. The results showed that anterior lung regions and posterior lung regions have lower and higher dose, respectively, for OTCM, compared to ATCM. For lung regions in the central line of AP direction, the lung doses are similar for OTCM and ATCM. Lungren *et al.* reported that the lung dose decreased by 7 % (average of 12 % and 2 %) and 13 % (average of 18 % and 7 %) for anterior and posterior lung regions, respectively.[16] In their study, the decrease of lung dose in posterior regions may be a result of sampling posterior lung dose more centrally compared to our sampling scheme.

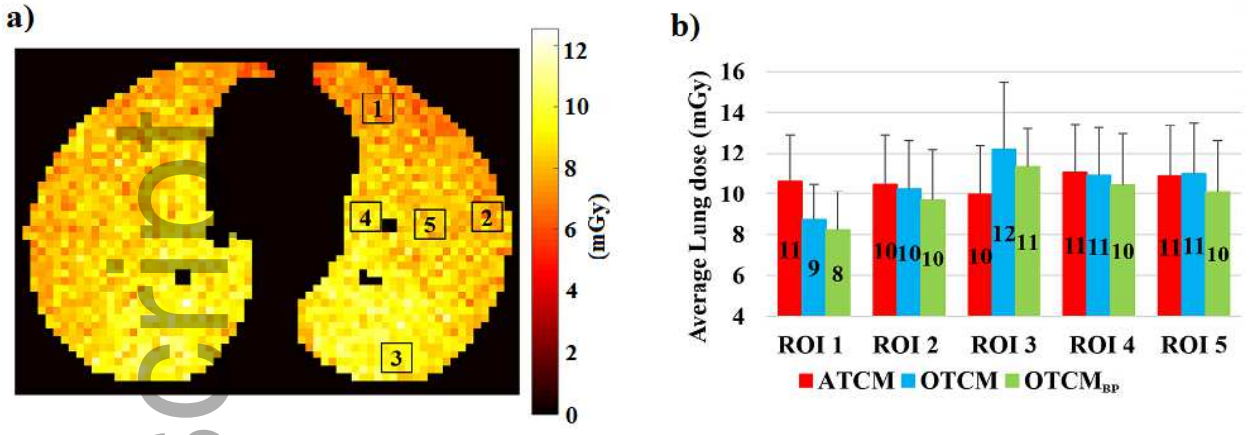


Figure 13: (a) Example of 5 ROIs drawn on dose distribution plots to evaluate the non-uniform distribution of lung dose. (b) For each ROI, the average dose value was calculated.

In this study, the primary focus was breast dose. However, the most relevant component of breast dose is average glandular dose (AGD). A side study was conducted to ascertain how the two are related. A prior study has derived the AGD from homogeneous breast tissue via simulation.[48] For each photon-material interaction, the dose to breast tissue was corrected to the glandular tissue by the ratio of glandular to breast mass attenuation coefficients at that energy level.[48] Using this approach, a conversion was derived as

$$r_{breast-to-AGD} = \sum \frac{\frac{\mu}{\rho}(E_i, glandular)}{\frac{\mu}{\rho}(E_i, breast)} P(E_i), \quad (5)$$

where $P(E_i)$ is source energy spectrum, filtered by the bowtie filter, and $\frac{\mu}{\rho}(E_i, glandular)$ and $\frac{\mu}{\rho}(E_i, breast)$ are the mass attenuation coefficients for glandular and breast tissues at energy $E_i$, respectively. Assuming the spectrum's further filtering by patient body can be ignored, $r_{breast-to-AGD}$ was computed to be 1.015 and 1.031 for the 50/50 breast and 20/80 breast, respectively. This indicates the breast dose and ADG are closely correlated at CT energies. Figure 14 shows a plot of average glandular dose for OTCM$_{BP}$ vs. OTCM. Please note, homogeneous distribution of glandular dose is an approximation. Future study is warranted to simulate heterogeneous breast tissue.

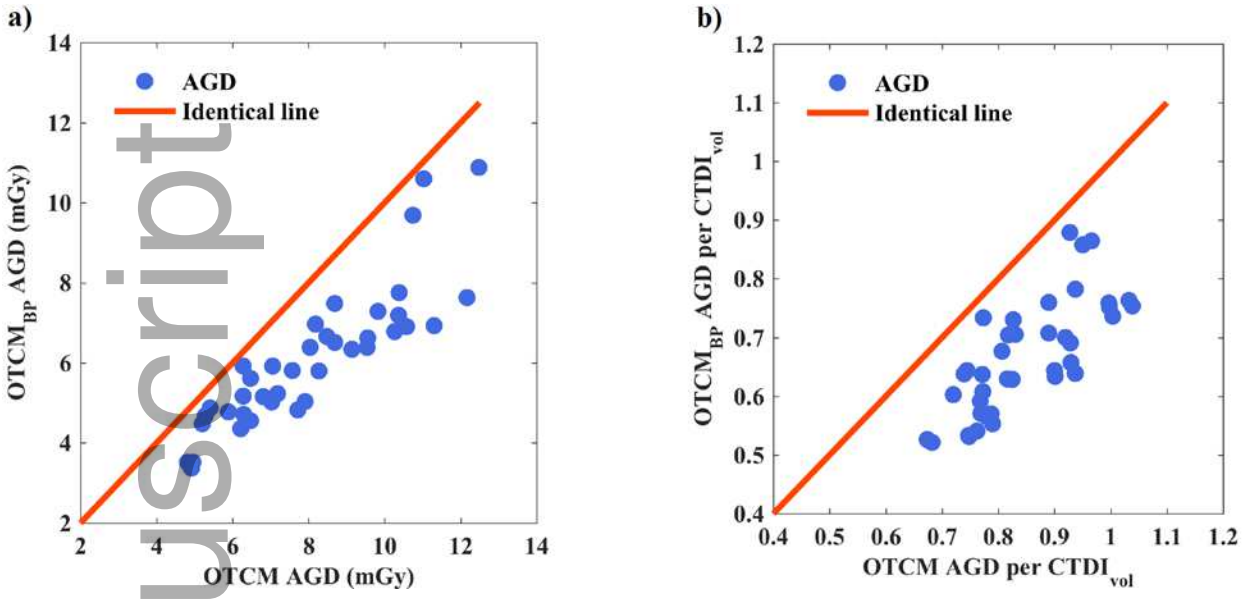


Figure 14: a) average glandular dose (AGD) and b) $CTDI_{vol}$-normalized-AGD simulated by $OTCM_{BP}$ vs. OTCM. The AGD was derived by equation (5).

This work has several limitations. First, the dose coefficient estimation was limited to one CT scanner. Second, although the dose reduction potential was demonstrated, an optimized positioning technique with minimum dose and patient comfort is yet to be defined. For each phantom, only one breast positioning was simulated. Third, image quality was not examined in this study. In previous studies, no significant difference in noise and CT numbers have been reported when comparing OTCM with ATCM or fixed mA scans using physical phantoms.[13, 14, 16] Neither were streaking and beam hardening artifacts with perceivable differences found. In Seidenfuss *et al.* work, the image quality was assessed for women scanned with OTCM, with and without a normal brassiere; no artifacts were reported.[44] A similar study will be conducted for $OTCM_{BP}$ in the future. Fourth, the mA profile was generated theoretically, as the actual mA in a CT system may not be predicted merely by patient attenuation.[24] For example, the mA profile may overshoot at the beginning of a scan.[49] To ensure the tube current profile in general agrees with the physical behavior, the skin dose was sampled and compared to studies measuring skin

dose on physical phantoms and our results showed strong agreement (Figure 12). Future studies may include modelling the mA profile taking into account actual physical behaviors. Fifth, the *h* factors and the comparisons for different modulation schemes reported in this study was specific to the mA scheme (average modulation strength). The study of other modulation strengths as well as other organ-based tube current modulation schemes used by various scanners and the associated effect on organ doses would be of value. However, as $CTDI_{vol}$ is a strong normalizing and a major factor significantly influencing organ dose, the $CTDI_{vol}$-normalized-organ dose dataset can reasonably characterize the net effect of modulation or breast positioning.

## CONCLUSION

In this study, the dose reduction potential of alternate breast positioning was evaluated for organ-based TCM examinations. Keeping $CTDI_{vol}$ constant, on average, compared to ATCM, OTCM reduced the breast dose by ~20 %. The average breast dose was further decreased by an additional 23 % with targeted breast positioning. Targeted breast positioning is needed to take full advantage of OTCM for reducing breast dose in body CT examinations.


## Acknowledgement

The authors would like to thank Juan Carlos Ramirez Giraldo for valuable discussions about the organ based tube current modulation technique.


## Disclosure of Conflicts of Interest

E.S. has grant support unrelated to this study from Siemens Medical Solutions and GE Healthcare. Other authors have no relevant conflicts of interest to disclose.

## REFERENCE


1 IMV, "CT Market Outlook Report," 2014).

2 R.G. Evens, F. Mettler, "National CT use and radiation exposure: United States 1983," American journal of roentgenology **144**, 1077-1081 (1985).

[3] D.J. Brenner, E.J. Hall, "Computed Tomography — An Increasing Source of Radiation Exposure," New England Journal of Medicine **357**, 2277-2284 (2007).

[4] C.H. McCollough, G.H. Chen, W. Kalender, S. Leng, E. Samei, K. Taguchi, G. Wang, L. Yu, R.I. Pettigrew, "Achieving routine submillisievert CT scanning: report from the summit on management of radiation dose in CT," Radiology **264**, 567-580 (2012).

[5] S.V. Vollmar, W.A. Kalender, "Reduction of dose to the female breast in thoracic CT: a comparison of standard-protocol, bismuth-shielded, partial and tube-current-modulated CT examinations," European radiology **18**, 1674-1682 (2008).

[6] J. Wang, X. Duan, J.A. Christner, S. Leng, K.L. Grant, C.H. McCollough, "Bismuth shielding, organ-based tube current modulation, and global reduction of tube current for dose reduction to the eye at head CT," Radiology **262**, 191-198 (2012).

[7] J. Valentin, *The 2007 recommendations of the international commission on radiological protection*. (Elsevier Oxford, 2007).

[8] E. Angel, N. Yaghmai, C.M. Jude, J.J. DeMarco, C.H. Cagnon, J.G. Goldin, C.H. McCollough, A.N. Primak, D.D. Cody, D.M. Stevens, "Dose to radiosensitive organs during routine chest CT: effects of tube current modulation," AJR. American journal of roentgenology **193**, 1340 (2009).

[9] B.L. Fricke, L.F. Donnelly, D.P. Frush, T. Yoshizumi, V. Varchena, S.A. Poe, J. Lucaya, "In-plane bismuth breast shields for pediatric CT: effects on radiation dose and image quality using experimental and clinical data," American Journal of Roentgenology **180**, 407-411 (2003).

[10] D. McLaughlin, R. Mooney, "Dose reduction to radiosensitive tissues in CT. Do commercially available shields meet the users' needs?," Clinical radiology **59**, 446-450 (2004).

[11] T. Kubo, P.-J.P. Lin, W. Stiller, M. Takahashi, H.-U. Kauczor, Y. Ohno, H. Hatabu, "Radiation dose reduction in chest CT: a review," American journal of roentgenology **190**, 335-343 (2008).

[12] M. Raissaki, K. Perisinakis, J. Damilakis, N. Gourtsoyiannis, "Eye-lens bismuth shielding in paediatric head CT: artefact evaluation and reduction," Pediatric radiology **40**, 1748-1754 (2010).

[13] X. Duan, J. Wang, J.A. Christner, S. Leng, K.L. Grant, C.H. McCollough, "Dose reduction to anterior surfaces with organ-based tube-current modulation: evaluation of performance in a phantom study," American Journal of Roentgenology **197**, 689-695 (2011).

[14] J. Wang, X. Duan, J.A. Christner, S. Leng, L. Yu, C.H. McCollough, "Radiation dose reduction to the breast in thoracic CT: comparison of bismuth shielding, organ-based tube current modulation, and use of a globally decreased tube current," Medical physics **38**, 6084-6092 (2011).

[15] E. Samei, "Pros and cons of organ shielding for CT imaging," Pediatric radiology **44**, 495-500 (2014).

[16] M.P. Lungren, T.T. Yoshizumi, S.M. Brady, G. Toncheva, C. Anderson-Evans, C. Lowry, X.R. Zhou, D. Frush, L.M. Hurwitz, "Radiation dose estimations to the thorax using organ-based dose modulation," American Journal of Roentgenology **199**, W65-W73 (2012).

[17] S. Taylor, D.E. Litmanovich, M. Shahrzad, A.A. Bankier, P.A. Gevenois, D. Tack, "Organ-based Tube Current Modulation: Are Women's Breasts Positioned in the Reduced-Dose Zone?," Radiology **274**, 260-266 (2014).

[18] A.H.S. Lee, "Why is carcinoma of the breast more frequent in the upper outer quadrant? A case series based on needle core biopsy diagnoses.," The Breast **14**, 2 (2005).

[19] K.J. Hurt, M.W. Guile, J.L. Bienstock, H.E. Fox, E.E. Wallach, *The Johns Hopkins manual of gynecology and obstetrics*. (Lippincott Williams & Wilkins, 2012).

[20] W.P. Segars, J. Bond, J. Frush, S. Hon, C. Eckersley, C.H. Williams, J. Feng, D.J. Tward, J.T. Ratnanather, M.I. Miller, D. Frush, E. Samei, "Population of anatomically variable 4D XCAT adult phantoms for imaging research and optimization," Medical Physics **40**, 043701 (2013).

[21] W. Segars, M. Mahesh, T. Beck, E. Frey, B. Tsui, "Realistic CT simulation using the 4D XCAT phantom," Medical physics **35**, 3800-3808 (2008).

[22] W. Segars, G. Sturgeon, S. Mendonca, J. Grimes, B.M. Tsui, "4D XCAT phantom for multimodality imaging research," Medical physics **37**, 4902-4915 (2010).

[23] J. Valentin, "Basic anatomical and physiological data for use in radiological protection: reference values: ICRP Publication 89," Annals of the ICRP **32**, 1-277 (2002).

[24] X. Li, W.P. Segars, E. Samei, "The impact on CT dose of the variability in tube current modulation technology: a theoretical investigation," Physics in medicine and biology **59**, 4525 (2014).

[25] M. Yaffe, J. Boone, N. Packard, O. Alonzo-Proulx, S.-Y. Huang, C. Peressotti, A. Al-Mayah, K. Brock, "The myth of the 50-50 breast," Medical physics **36**, 5437-5443 (2009).

[26] G. Richard Hammerstein, D.W. Miller, D.R. White, M. Ellen Masterson, H.Q. Woodard, J.S. Laughlin, "Absorbed Radiation Dose in Mammography 1," radiology **130**, 485-491 (1979).

[27] X. Li, E. Samei, W.P. Segars, G.M. Sturgeon, J.G. Colsher, G. Toncheva, T.T. Yoshizumi, D.P. Frush, "Patient-specific radiation dose and cancer risk estimation in CT: Part I. Development and validation of a Monte Carlo program," Medical physics **38**, 397-407 (2011).

[28] J.A. Schnabel, C. Tanner, A.D. Castellano-Smith, A. Degenhard, M.O. Leach, D.R. Hose, D.L. Hill, D.J. Hawkes, "Validation of nonrigid image registration using finite-element methods: application to breast MR images," Medical Imaging, IEEE Transactions on **22**, 238-247 (2003).

[29] C. Tanner, A. Degenhard, J. Schnabel, A.C. Smith, C. Hayes, L. Sonoda, M. Leach, D. Hose, D. Hill, D. Hawkes, "A method for the comparison of biomechanical breast models," in *Mathematical Methods in Biomedical Image Analysis, 2001. MMBIA 2001. IEEE Workshop on* (IEEE, 2001), pp. 11-18.

[30] A.L. Kellner, T.R. Nelson, L.I. Cerviño, J.M. Boone, "Simulation of mechanical compression of breast tissue," Biomedical Engineering, IEEE Transactions on **54**, 1885-1891 (2007).

[31] C.M. Hsu, M.L. Palmeri, W.P. Segars, A.I. Veress, J.T. Dobbins III, "An analysis of the mechanical parameters used for finite element compression of a high-resolution 3D breast phantom," Medical physics **38**, 5756-5770 (2011).

[32] S.A. Maas, B.J. Ellis, G.A. Ateshian, J.A. Weiss, "FEBio: finite elements for biomechanics," Journal of biomechanical engineering **134**, 011005 (2012).

[33] X. Li, E. Samei, W.P. Segars, G.M. Sturgeon, J.G. Colsher, G. Toncheva, T.T. Yoshizumi, D.P. Frush, "Patient-specific radiation dose and cancer risk estimation in CT: part II. Application to patients," Medical physics **38**, 408-419 (2011).

[34] J. Baro, J. Sempau, J. Fernández-Varea, F. Salvat, "PENELOPE: an algorithm for Monte Carlo simulation of the penetration and energy loss of electrons and positrons in matter," Nuclear Instruments and Methods in Physics Research Section B: Beam Interactions with Materials and Atoms **100**, 31-46 (1995).

[35] J. Sempau, J. Fernandez-Varea, E. Acosta, F. Salvat, "Experimental benchmarks of the Monte Carlo code PENELOPE," Nuclear Instruments and Methods in Physics Research Section B: Beam Interactions with Materials and Atoms **207**, 107-123 (2003).

[36] X. Tian, X. Li, W.P. Segars, E.K. Paulson, D.P. Frush, E. Samei, "Pediatric Chest and Abdominopelvic CT: Organ Dose Estimation Based on 42 Patient Models," Radiology **270**, 535-547 (2014).

[37] X. Li, E. Samei, W.P. Segars, G.M. Sturgeon, J.G. Colsher, D.P. Frush, "Patient-specific radiation dose and cancer risk for pediatric chest CT," Radiology **259**, 862-874 (2011).

[38] X. Tian, X. Li, W.P. Segars, D.P. Frush, E. Samei, "Prospective estimation of organ dose in CT under tube current modulation," Medical physics **42**, 1575-1585 (2015).

[39] AAPM, Report No. 220, 2014.

[40] AAPM, Report No. 204, 2011.

[41] R. Protection, "ICRP publication 103," Ann. ICRP **37**, 2 (2007).

[42] P. Sahbaee, W.P. Segars, E. Samei, "Patient-based estimation of organ dose for a population of 58 adult patients across 13 protocol categories," Medical physics **41**, 072104 (2014).

[43] A.C. Turner, D. Zhang, M. Khatonabadi, M. Zankl, J.J. DeMarco, C.H. Cagnon, D.D. Cody, D.M. Stevens, C.H. McCollough, M.F. McNitt-Gray, "The feasibility of patient size-corrected, scanner-independent organ dose estimates for abdominal CT exams," Medical physics **38**, 820-829 (2011).

[44] A. Seidenfuss, A. Mayr, M. Schmid, M. Uder, M.M. Lell, "Dose Reduction of the Female Breast in Chest CT," American Journal of Roentgenology **202**, W447-W452 (2014).

[45] B.J. O'Hea, A.D. Hill, A.M. El-Shirbiny, S.D. Yeh, P.P. Rosen, D.G. Coit, P.I. Borgen, H.S. Cody, "Sentinel lymph node biopsy in breast cancer: initial experience at Memorial Sloan-Kettering Cancer Center," Journal of the American College of Surgeons **186**, 423-427 (1998).

[46] M.T. Dixon, R.J. Loader, G.C. Stevens, N.P. Rowles, "An evaluation of organ dose modulation on a GE optima CT660-computed tomography scanner," Journal of Applied Clinical Medical Physics **17**2016).

[47] P.D. Darbre, "Recorded quadrant incidence of female breast cancer in Great Britain suggests a disproportionate increase in the upper outer quadrant of the breast," Anticancer research **25**, 2543-2550 (2005).

[48] J.M. Boone, T.R. Nelson, K.K. Lindfors, J.A. Seibert, "Dedicated breast CT: Radiation dose and image quality evaluation 1," Radiology **221**, 657-667 (2001).

[49] M. Khatonabadi, H.J. Kim, P. Lu, K.L. McMillan, C.H. Cagnon, J.J. DeMarco, M.F. McNitt-Gray, "The feasibility of a regional CTDIvol to estimate organ dose from tube current modulated CT exams," Medical physics **40**, 051903 (2013).

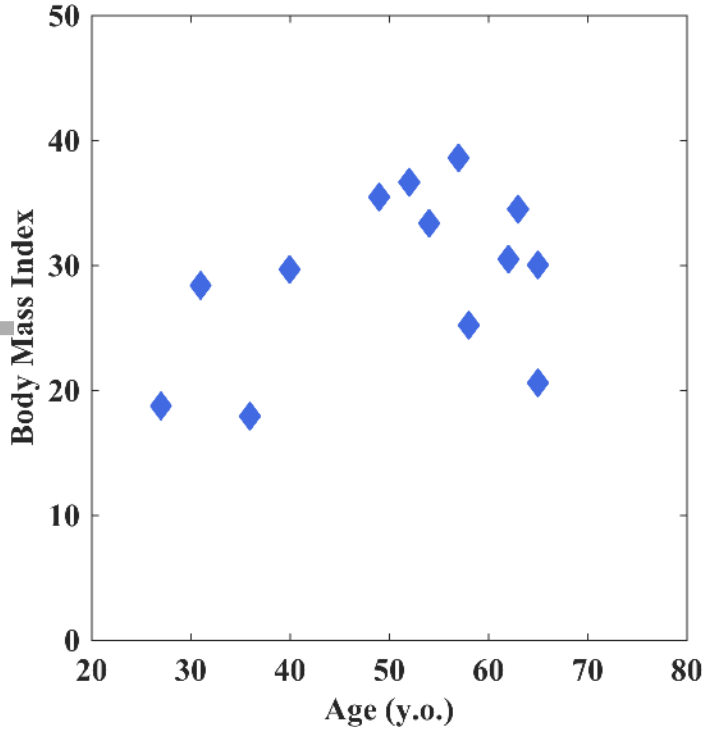


mp_12076_f1.tif

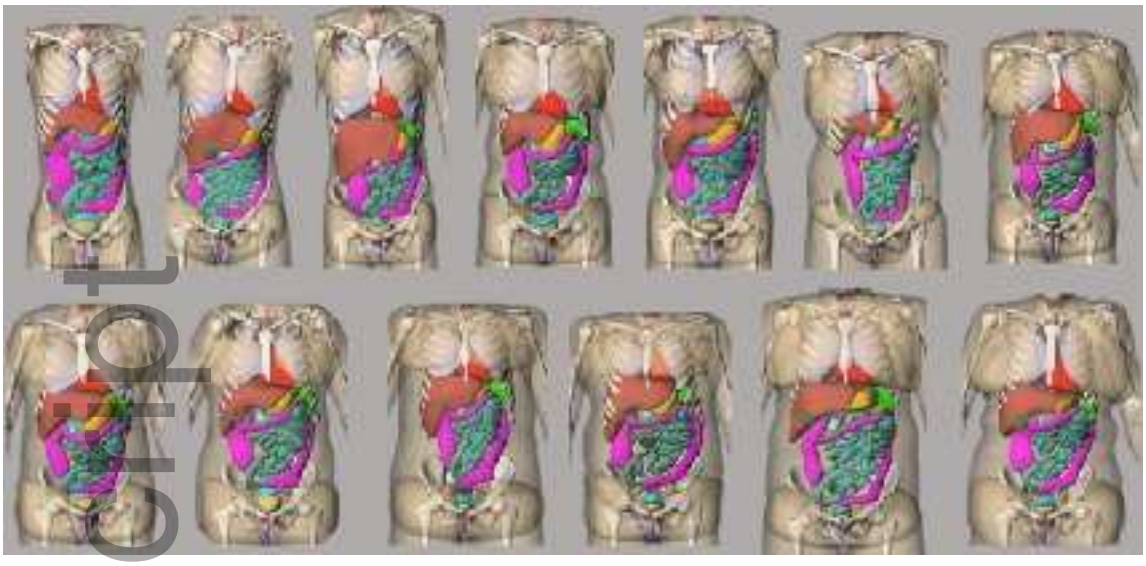

mp_12076_f2.tif

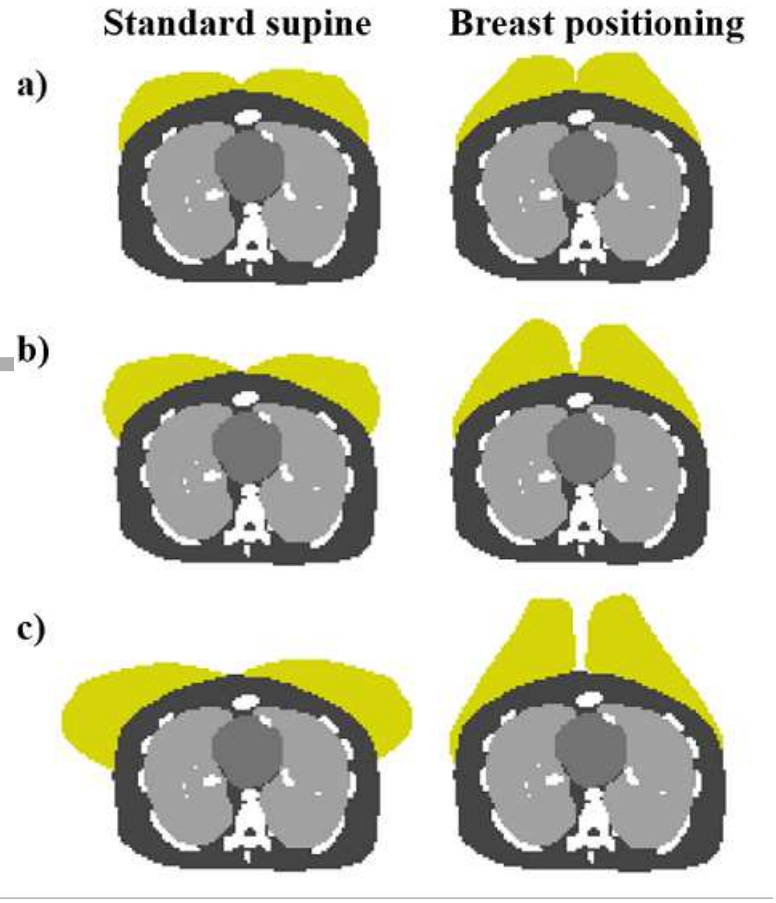


mp_12076_f3.tif

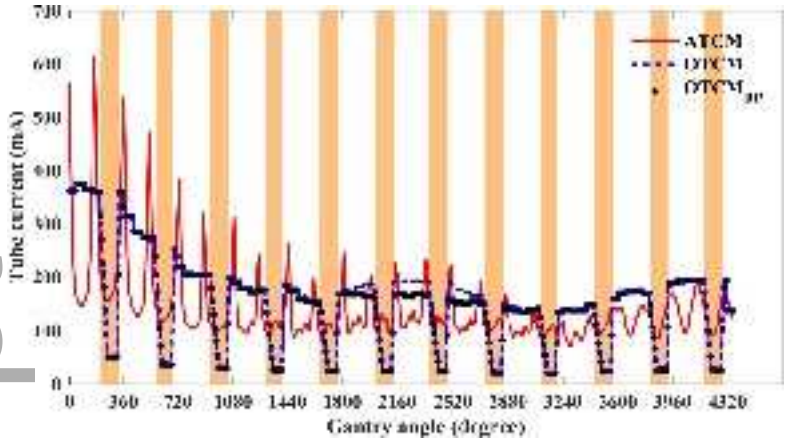


mp_12076_f4.tif

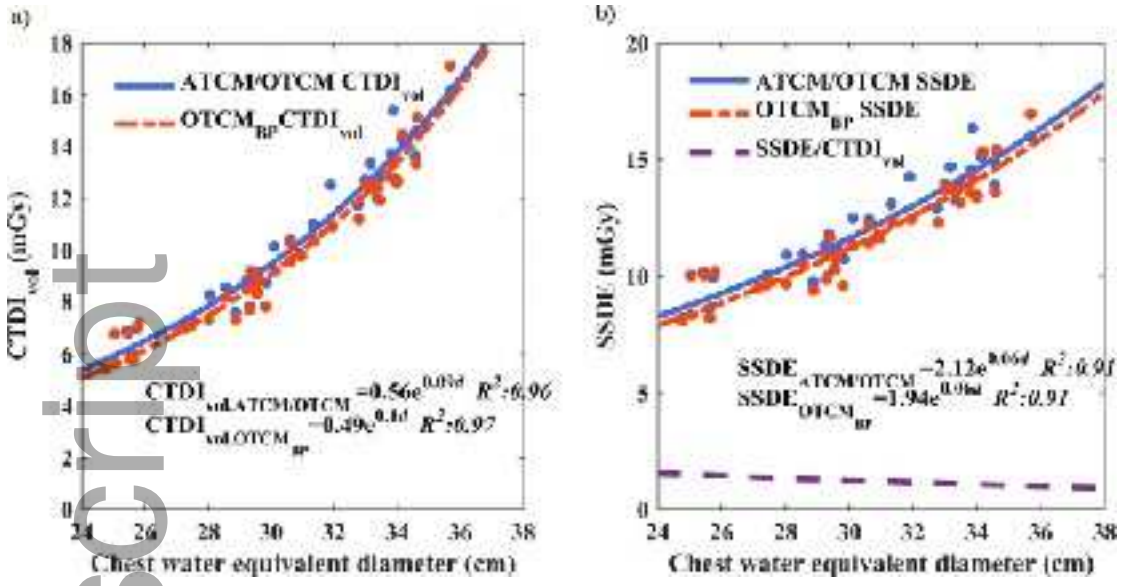


mp_12076_f5.tif

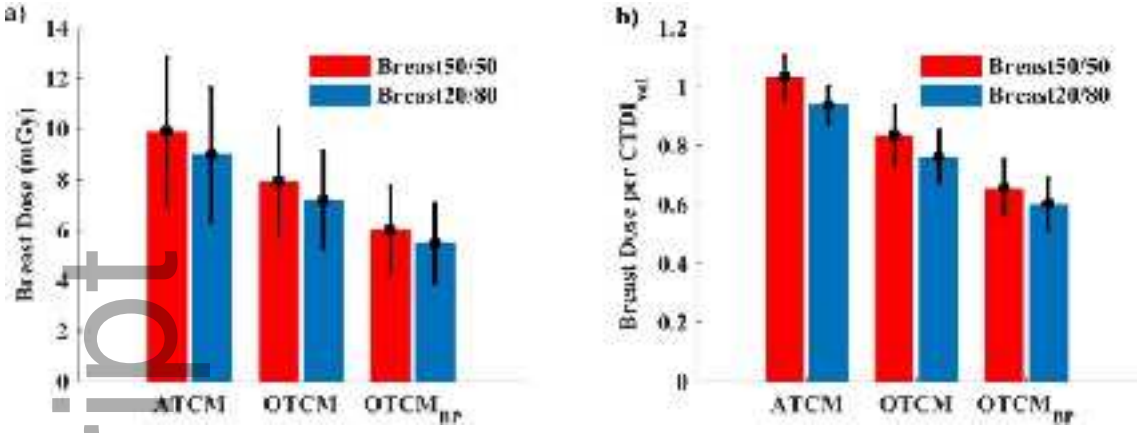


mp_12076_f6.tif

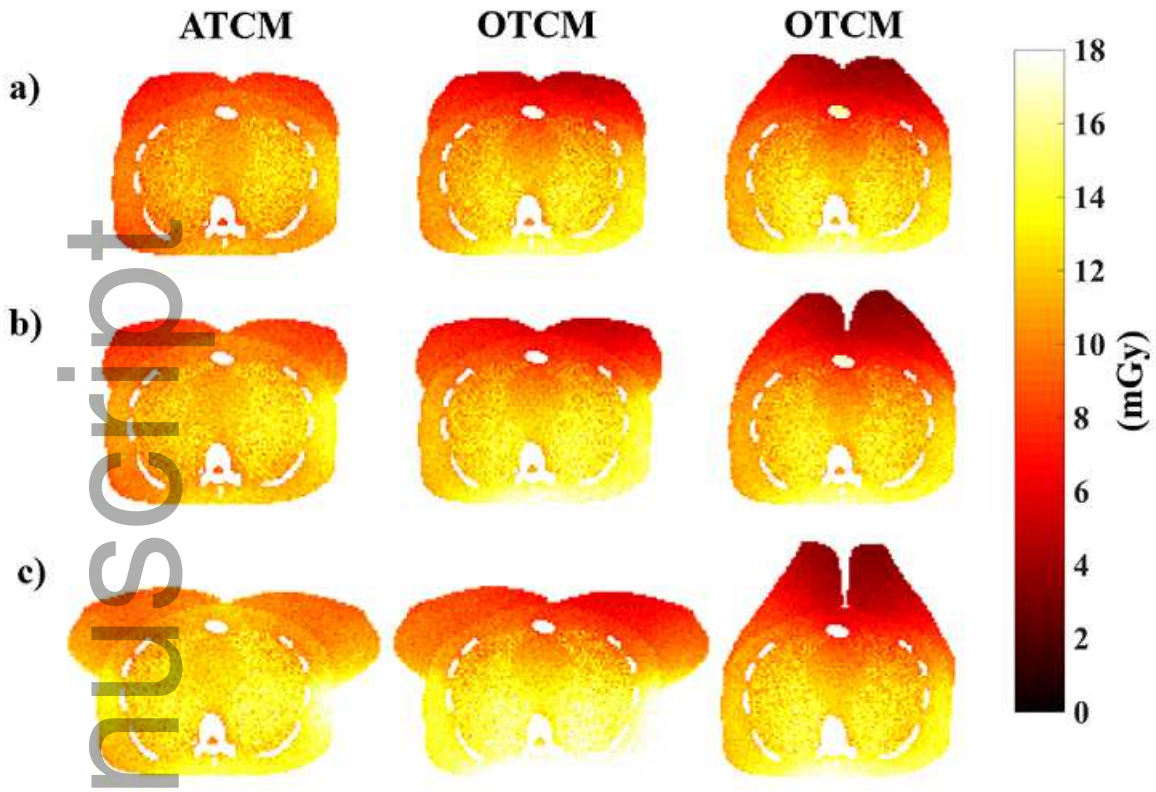


mp_12076_f7.tif

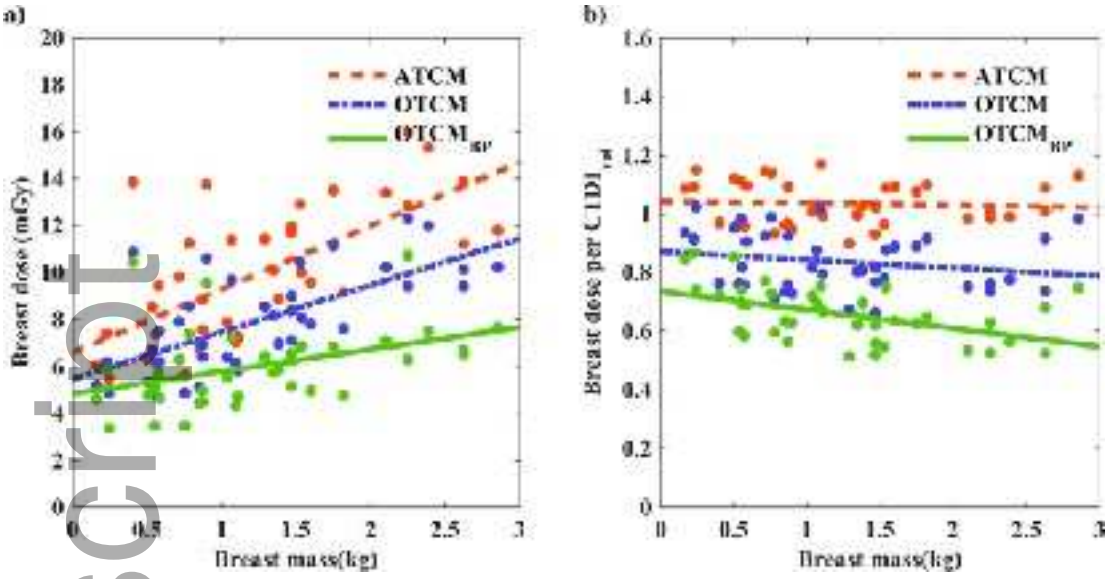


mp_12076_f8.tif

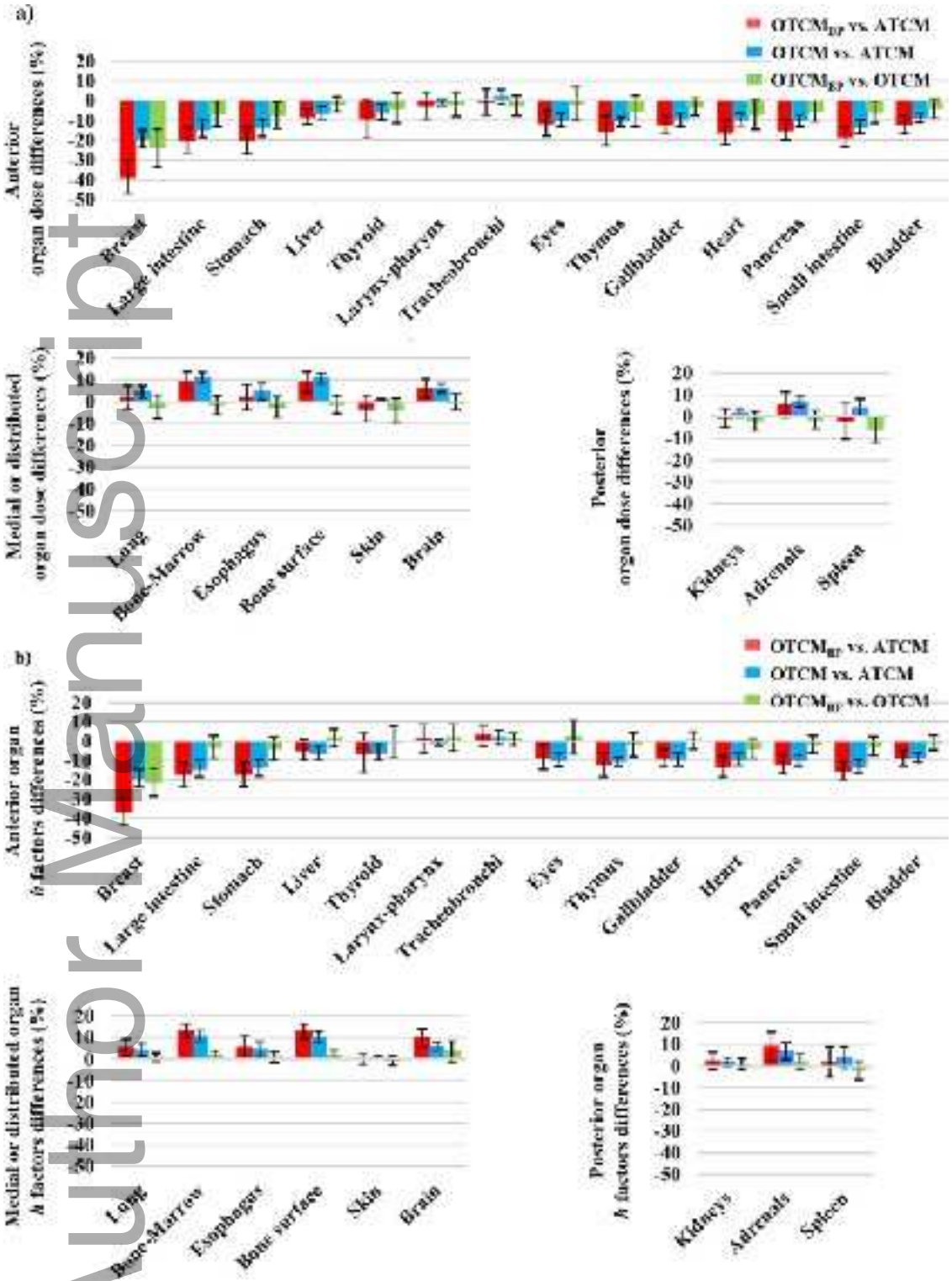


mp_12076_f9.tif

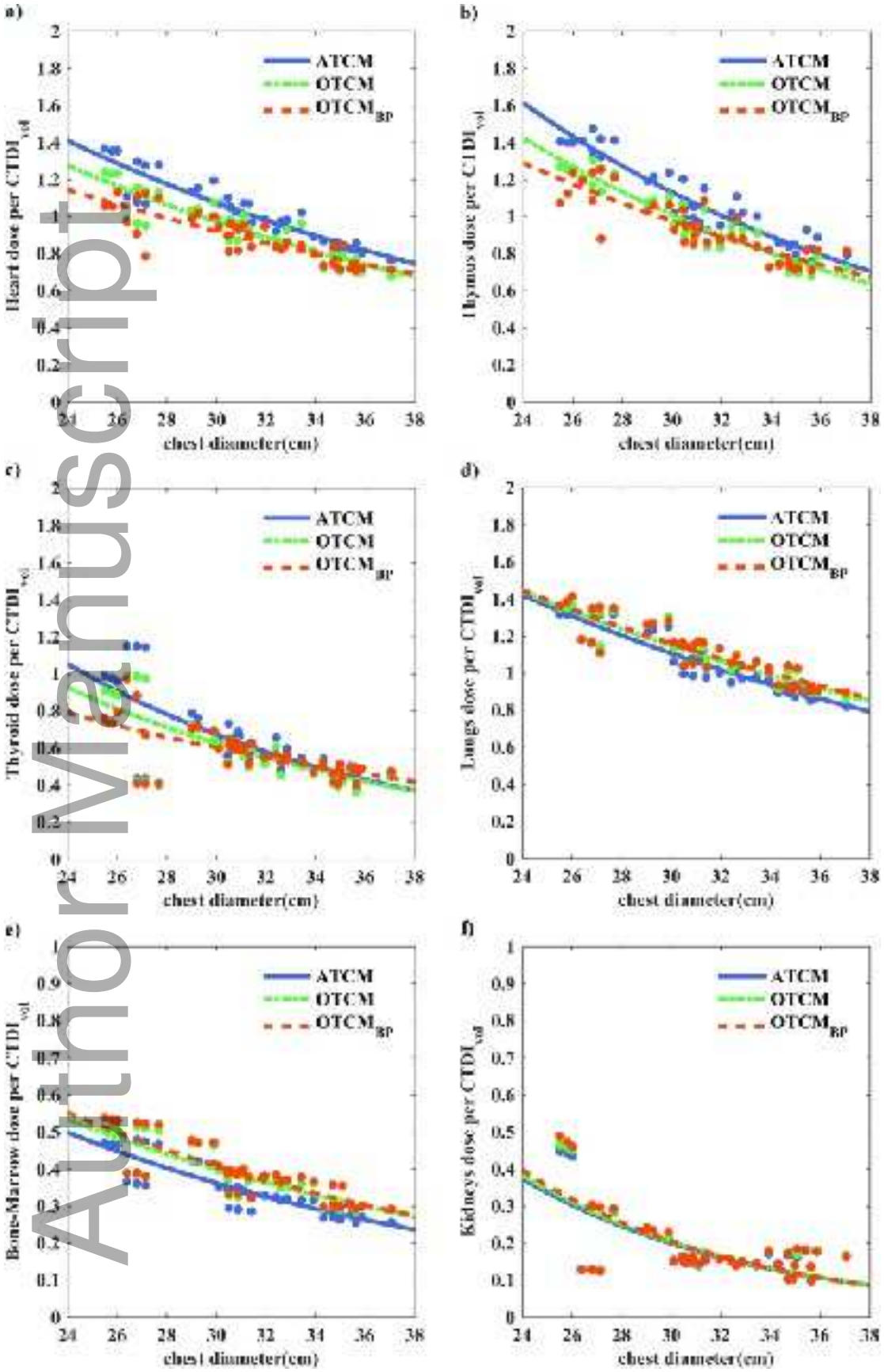


mp_12076_f10.tif

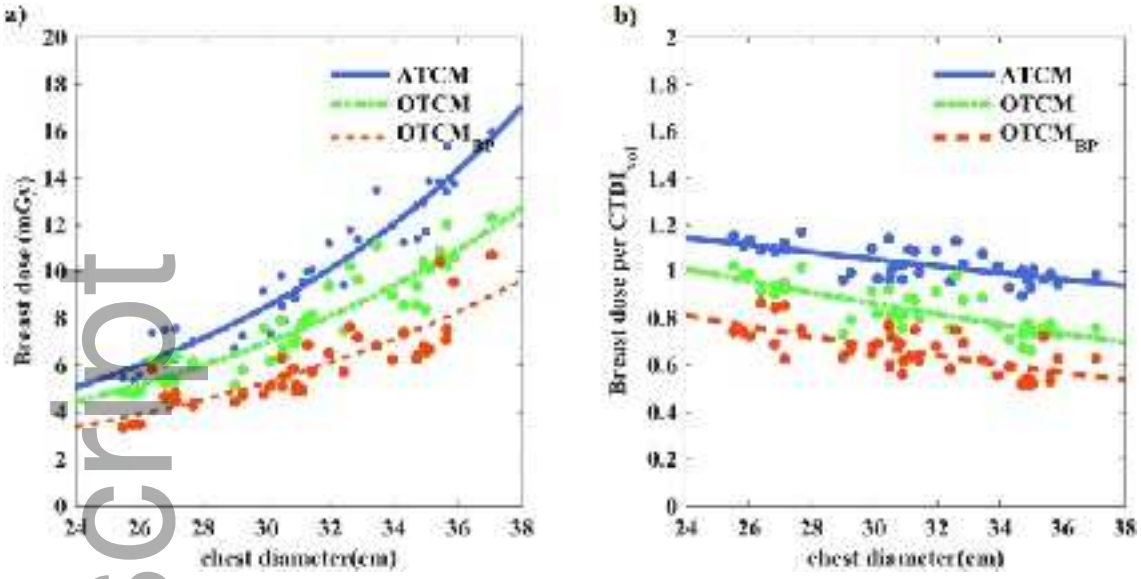


mp_12076_f11.tif

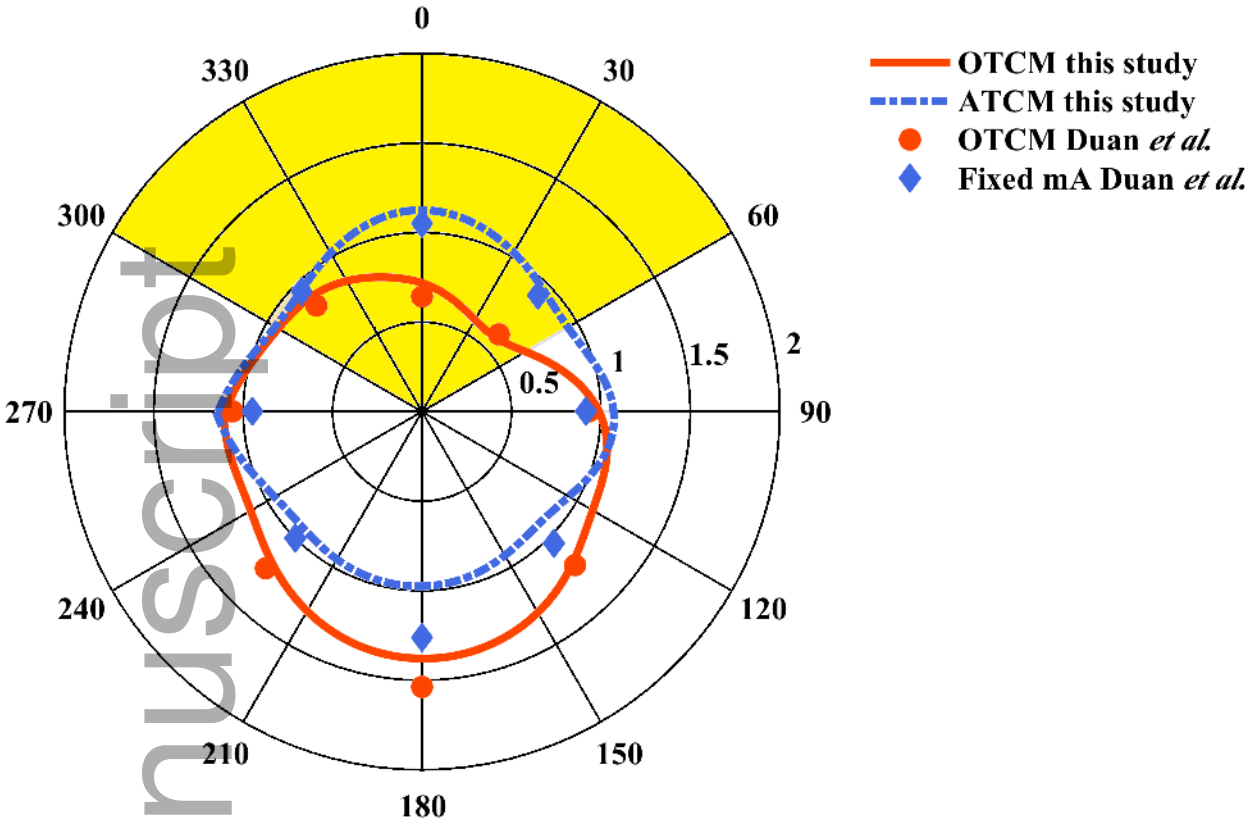


mp_12076_f12.tif

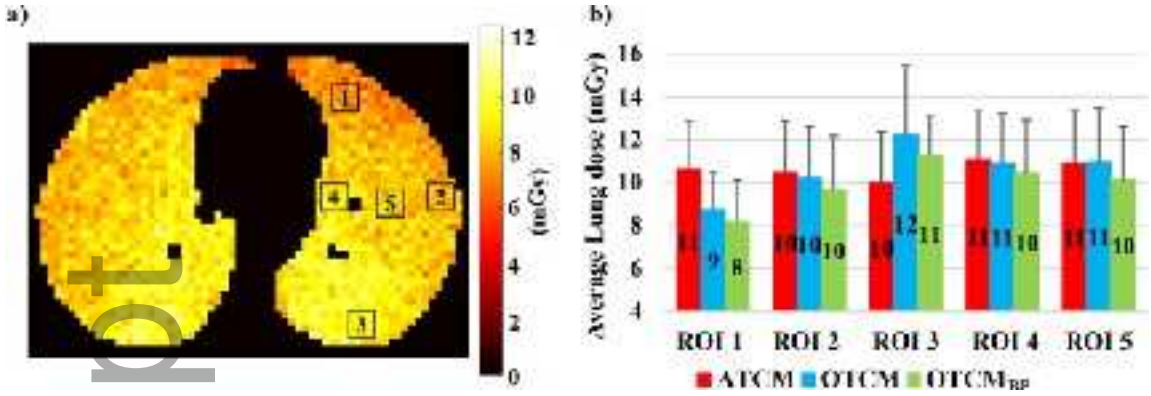


mp_12076_f13.tif

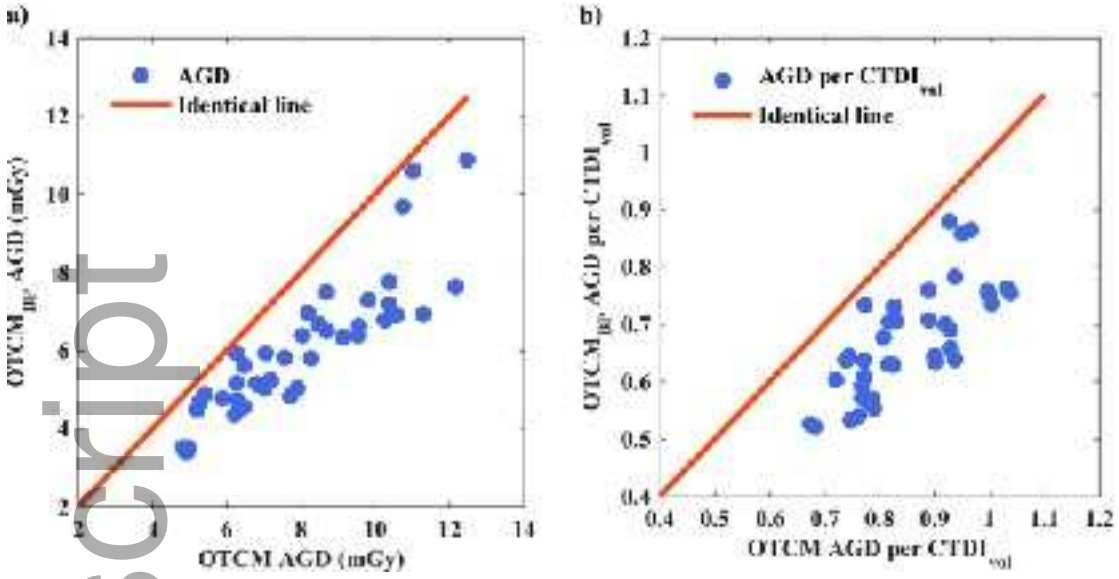


mp_12076_f14.tif